Atmos. Chem. Phys. Discuss., 8, 14643–14716, 2008
www.atmos-chem-phys-discuss.net/8/14643/2008/

Atmospheric Chemistry and Physics Discussions

This discussion paper is/has been under review for the journal *Atmospheric Chemistry and Physics (ACP)*. Please refer to the corresponding final paper in *ACP* if available.

Isoprene photooxidation mechanism: resonance channels and implications for the production of nitrates and acids

F. Paulot[1], J. D. Crounse[2], H. G. Kjaergaard[3], J. H. Kroll[2,4], J. H. Seinfeld[1,2], and P. O. Wennberg[1,5]

[1]Division of Environmental Science and Engineering, California Institute of Technology, Pasadena, CA, USA
[2]Division of Chemistry and Chemical Engineering, California Institute of Technology, Pasadena, CA, USA
[3]Department of Chemistry, University of Otago, Dunedin, New Zealand
[4]Center for Aerosol and Cloud Chemistry, Aerodyne Inc., Billerica, MA, USA
[5]Division of Geophysical and Planetary Sciences, California Institute of Technology, Pasadena, CA, USA

Received: 10 June 2008 – Accepted: 2 July 2008 – Published: 31 July 2008

Correspondence to: F. Paulot (paulot@caltech.edu)

Published by Copernicus Publications on behalf of the European Geosciences Union.

Abstract

We describe a nearly explicit chemical mechanism for isoprene photooxidation guided by chamber studies that include time-resolved observation of an extensive suite of volatile compounds. We provide new constraints on the chemistry of the poorly-understood isoprene resonance channels, which account for more than one third of the total isoprene carbon flux and a larger fraction of the nitrate yields. We show that the cis branch dominates the chemistry of the isoprene resonance channel with less than 5% of the carbon following the trans branch. We find that the yield of isoprene nitrates is approximately 11%. The oxidation of these nitrates releases nearly 50% of the NO_x. Methacrolein nitrates (15% yield) and methylvinylketone nitrates (10% yield) are also observed. Propanone nitrate is produced with a yield of 1% and appears to be the longest-lived nitrate formed in the total oxidation of isoprene. We find a large molar yield of formic acid and suggest a novel mechanism leading to its formation from the organic nitrates. Finally, the most important features of this mechanism are summarized in a condensed scheme appropriate for inclusion in global chemical transport models.

1 Introduction

Isoprene (2-methyl-1,3-butadiene, C_5H_8) is a short-lived compound ($\tau_{1/2}$=1–2 h) emitted by many deciduous trees during daylight hours. Between 0.5% and 2% of the carbon fixed by plants that emit isoprene is released to the atmosphere as isoprene (Harley et al., 1999), a flux accounting for about one third of the total anthropogenic and natural volatile organic compounds (VOC) emissions (Guenther et al., 2006). Isoprene plays a crucial role in determining the oxidative chemistry of the troposphere. Ozone levels in urban as well as in rural sites are impacted by the sequestration and transport of NO_X via formation of isoprene nitrates (Horowitz et al., 1998) and various isoprene-derived peroxyacylnitrates. Moreover, field (Claeys et al., 2004) and chamber

studies (Kroll et al., 2006; Surratt et al., 2006) have recently shown that compounds formed in isoprene photooxidation, such as methylglyceric acid or methylerythritol are ubiquitous in aerosol particles and may contribute significantly to the aerosol global burden (Henze and Seinfeld, 2006; van Donkelaar et al., 2007).

In the light of the potential for significant change in isoprene emissions due to climate and land use changes (Shallcross and Monks, 2000), studies have been made to quantify the impact of altered isoprene emissions on tropospheric ozone (Sanderson et al., 2003; Wiedinmyer et al., 2006). von Kuhlmann et al. (2004) and Fiore et al. (2005) note, however, that quantifying this impact is difficult due to uncertainties regarding: 1) the dependence of isoprene emissions on temperature (Harley et al., 2004) and the CO_2 concentration (Rosenstiel et al., 2003); and 2) the isoprene photooxidation scheme, especially the yields and fates of isoprene nitrates.

In this study, we use a state of the art chemical ionization mass spectrometry (CIMS) technique (Crounse et al., 2006) to monitor, in real-time, a wide variety of compounds formed during isoprene photooxidation in an atmospheric chamber. Combined with a newly developed chemical mechanism, these detailed observations help us unravel some of the main features of the isoprene photooxidation mechanism. Here we focus on studies made with NO_X present in initial excess.

First, we describe the basic chemical rules which shape the mechanism. Then we examine in detail the first stages of isoprene photooxidation, focusing on the resonance channel, the organic nitrate yield and fate, as well as some routes to organic acids. Finally, we derive the molar yields for a suite of compounds and present a reduced mechanism.

2 Experiments

2.1 Experimental setting

The data in the present study are based on an experiment carried out in the 28 m^3 Caltech atmospheric chamber similar to the one described by Kroll et al. (2006). Initial concentrations of isoprene, NO and H_2O_2 were 94 ppbv, 500 ppbv and 2.1 ppmv. The photolysis of H_2O_2 constitutes the primary source of HO in the experiment. NO was added prior to isoprene so that the chamber was initially ozone free. The initial relative humidity was less than 6% and is assumed to be constant in this study. The temperature increased by about 5 degrees in the first one hundred minutes and remained constant at 296.5 K for the rest of the run. To simplify the analysis, we considered this temperature to hold during the whole experiment.

The size distribution and the volume concentration of secondary organic aerosol (SOA) was measured using a differential mobility analyzer (DMA, TSI 3760). Further details are available in Kroll et al. (2006).

2.2 CIMS

Gas-phase products, including acids, were monitored using a novel CIMS technique (Crounse et al., 2006). Air was drawn from the chamber through a perfluoroalkoxy Teflon line of 1.2 m length and 0.635 cm outer diameter (OD), at a rate of 10 standard liters per minute (slpm), and then sub-sampled into the CIMS flow tube using a critical orifice made of glass. The orifice constrained the flow from the chamber into the CIMS to be 145 standard cubic centimeters per minute (sccm). Upon introduction to the CIMS flow tube, the chamber gas was diluted with 1760 sccm of UHP N_2 (99.999%) to a total pressure of 35 hPa, primarily to reduce the concentration of H_2O_2 to manageable levels. The CIMS flow tube was made of 2.54 cm OD Pyrex glass which was coated with a thin layer of Teflon (Fluoropel 801A, from Cytonix Corp.). The flow tube extended 17.8 cm beyond the transverse ion beam (Crounse et al., 2006, Fig. 1), and was re-

duced to 0.635 cm OD on the upstream end to allow connection of the input gasses. Mass scans were conducted using a quadrupole mass spectrometer from m/z=18 to m/z=275 dwelling on each mass for 1 s (giving a scan cycle of about $4\frac{1}{2}$ min). The mass scans were repeated throughout the duration of the experiments (8–20 h). Zero scans were conducted periodically throughout the experiment by overfilling the critical orifice on the high pressure (chamber) side with UHP N_2. In addition to providing instrumental backgrounds, the temporal response of the zero scans give insight into the strength of the interaction of the measured compounds with the equipment walls.

Unreactive with ozone, carbon dioxide and dioxygen (Huey et al., 1996), the reagent ion, CF_3O^-, is shown to be very useful for the detection of many oxygenated compounds generated through atmospheric photo-oxidation reactions of organic and inorganic compounds, as will be shown throughout this work. In general, two primary ionization pathways are observed:

$$VOC + CF_3O^- \rightarrow VOC\_H^- \cdot HF + CF_2O \quad (R1)$$

$$VOC + CF_3O^- \leftrightarrows VOC \cdot CF_3O^- \quad (R2)$$

A minor ionization pathway is observed for certain compounds:

$$CF_3O^- + HOOX(O)R \rightarrow HF + CF_2O \cdot OOX(O)R^- \quad (R3)$$

In Reaction (R3), CF_2O is incorporated into the original neutral molecule. Reaction (R3) has been observed for peroxynitric acid (PNA) and for peroxy acetic acid (PAA). Quantum mechanical calculations are necessary to elucidate the exact structure of these product ions. While Reaction (R3) is not the major ionization pathway, it is useful as a fingerprint to distinguish mass analogs.

The dominant ionization pathway for a neutral analyte depends mostly on the acidity (or fluoride affinity) of the neutral species (Amelynck et al., 2000; Crounse et al., 2006). Highly acidic compounds, such as nitric acid, only form the transfer product ion throught Reaction (R1) while hydrogen peroxide and methylhydrogen peroxide (MHP) form only the cluster product ion throught Reaction (R2). Species with intermediate acidity (e.g. formic and acetic acids) form both the transfer and cluster products.

2.3 Calibration

The concentration of a compound X, whose product ion is detected at m/z=p, can be calculated through:

$$[X]_{ppbv} = \frac{\widehat{Signal(m/z=p)}}{c_X} \quad (1)$$

where $\widehat{Signal(m/z=p)}$ is the normalized signal associated with X (cf. Appendix B1) and c_X is the calibration for the compound X in $ppbv^{-1}$.

For most compounds, no experimental determination of c_X has been made. In such cases, we assume that c_X is related to the thermal capture rate (k_X) and the binding energy of the cluster.

k_X is estimated from the Langevin-Gioumousis-Stevenson-based collision rate through the dipole moment (μ_X) and the polarizability (α_X) of X using the empirical approach developed by Su and Chesnavich (1982).

Since experimental determinations of both properties are lacking for most of the isoprene photooxidation products, we have used quantum chemical calculations to obtain these. The lowest energy conformers of the molecules were found with the conformer searches method within the Spartan06 quantum package (Wavefunction Inc., 2006). The dipoles and static polarizabilities are then calculated for the optimized geometries with the B3LYP/6-31G(d) method. When a molecule has several low energy conformers, a weighted average of their reaction rates is used for k_X (cf. Appendix B2 for details).

The sensitivity of the instrument to X also depends on the binding energy between X and the reagent anion as well as the nature of the reagent anion. In the presence of abundant ligands (L) such as water or hydrogen peroxide, the sensitivity of the CIMS to some VOC is modified through two different processes: 1) $CF_3O^- \cdot L$ may react faster with X than the bare anion because of ligand exchange reactions stabilizing the product ion to a greater extent; 2) the cluster $CF_3O^- \cdot L$ may be sufficiently stable leading to a

lower sensitivity at higher L mixing ratio due to ligand exchange.

$$\mathrm{VOC.CF_3O^-} + L \leftrightarrows \mathrm{VOC} + \mathrm{L{\cdot}CF_3O^-} \quad \text{(R4)}$$
$$\mathrm{L} = \mathrm{H_2O}, \mathrm{H_2O_2}$$

For example, Crounse et al. (2006) reported that the sensitivity to methylperoxide decreases with the water vapor mixing ratio due to Reaction (R4).

Larger molecules, i.e. molecules with more than three heavy atoms featuring a nitrate group, a peroxide group, or a carbonyl and an hydroxide exhibit only a weak dependence on water. This is also the case for strong acids such as HNO_3. Therefore, we neglect the binding energy effect in this study and take:

$$c_X = \frac{k_X}{k_{\mathrm{HNO_3}}} c_{\mathrm{HNO_3}} \quad (2)$$

where $k_{\mathrm{HNO_3}}$=1.93×10^{-9} cm^3 molecule^{-1} s^{-1} is calculated using the experimental dipole and polarizability of nitric acid and $c_{\mathrm{HNO_3}}$ is the sensitivity to nitric acid for typical conditions where the flow tube was operated (water vapor mixing ratio =150 ppmv). HNO_3 is used as the calibration reference because of the weak dependence of the sensitivity with water and its thorough laboratory study (Huey et al., 1996; Amelynck et al., 2000; Crounse et al., 2006).

When several compounds are observed at the same m/z, we report the signal calibrated with a reference calibration c_{ref} (cf. Appendix B) and the modeled concentrations of each compound multiplied by s_X=c_X/c_{ref}.

Finally, molecules such as isoprene, methacrolein (MACR, acronyms are listed in Table C) and methylvinylketone (MVK) are not observed with our measurement technique despite their average dipole moment. More generally, the method is not sensitive to simple aldehydes, alcohols, and ketones, presumably due to the low binding energy of these compounds with CF_3O^-.

3 Photooxidation mechanism

3.1 VOC chemistry

Except as noted below, we use the known rate coefficients of bimolecular and termolecular reactions as tabulated in IUPAC (Atkinson et al., 2004, 2006) and JPL (Sander, 2006) reports.

3.1.1 HO

Reactions of HO with VOC are limited to its addition on a double bond and the abstraction of the aldehydic hydrogen and the hydrogen in α of an alcohol, i.e. the abstraction of hydrogens from alcohols is neglected. For the addition of HO onto double bonds, in the absence of data or previous information enabling differentiation between the two carbons, we assume that the reaction occurs only on the most favorable location based on steric considerations. A structure-activity relationship (SAR) method is used to determine unknown reaction rates (Kwok and Atkinson, 1995).

Following the studies of Orlando and Tyndall (2001) and Méreau et al. (2001), acyl-radicals are assumed to decompose promptly when the alkyl group is tertiary or features a carbonyl in α of the radical:

$$\mathrm{R_1R_2R_3CCHO} + \mathrm{HO} \rightarrow \mathrm{R_1R_2R_3CCO} + \mathrm{H_2O} \quad \text{(R5)}$$
$$\mathrm{R_1R_2R_3CCO} \rightarrow \mathrm{R_1R_2R_3C} + \mathrm{CO} \quad \text{(R6)}$$

In all other cases, the acyl radical is assumed to add O_2 to yield the associated peroxy radical.

3.1.2 Ozone

Ozone reacts with alkenes via the formation of a molozonide, quickly followed by its decomposition into a carbonyl and a Criegee intermediate. Assuming a generic rate

constant for the reaction of alkenes with ozone, 10^{-17} cm^3 molecule^{-1} s^{-1} , the reaction of an alkene with ozone is included if $\tau_{HO} > \frac{\tau_{O_3}}{10}$, where τ_{HO} and τ_{O_3} are the lifetimes of the alkenes with respect to HO and O_3 respectively.

Ozone reactions are included for isoprene, MACR and MVK, following IUPAC recommendations.

3.1.3 NO_3

Reactions of NO_3 with alkenes and aldehydes have been neglected, since $\frac{k^{NO_3}_{\{alkenes/aldehydes\}}[NO_3]}{k^{HO}_{\{alkenes/aldehydes\}}[HO]} \ll 1$ throughout the experiment

3.2 Peroxyradical chemistry

3.2.1 NO

NO reacts with peroxy radicals with a rate coefficient of $2.43 \times 10^{-12} \exp(360/T)$ cm^3 molecule^{-1} s^{-1} (Atkinson et al., 2006) through

$$RO_2 + NO \rightarrow (1 - \alpha)(RO + NO_2) + \alpha RONO_2 \quad \text{(R7)}$$

A reaction rate coefficient of $6.7 \times 10^{-12} \exp(340/T)$ cm^3 molecule^{-1} s^{-1} is used for acyl peroxy based on $CH_3CH_2C(O)OO$.

Carter's parameterization is used to compute the alkyl nitrate yield (Carter and Atkinson, 1989; Arey et al., 2001):

$$\frac{\alpha}{1-\alpha} = \frac{Y_0^{298}[M](T/298)^{-m_0}}{1+\Theta} F^Z \times m \quad (3)$$

with $z = (1 + [\log(\frac{Y_o^{298}[M](T/298)^{-m_0}}{Y_\infty^{298}[M](T/298)^{-m_\infty}})]^2)^{-1}$, $F = 0.41$, $m_0 = 0$, $m_\infty = 8.0$, $\beta = 1$, $\Theta = \frac{Y_0^{298}[M](T/298)^{-m_0}}{Y_\infty^{298}(T/298)^{-m_\infty}}$, $\gamma = 2 \times 10^{-22}$ cm^{3}molecule^{-1}, $Y_\infty^{298} = 0.43$, $Y_0^{298} = \gamma e^{\beta n}$, where n

is the number of carbons in the molecule. The parameter m is set to 0.4, 1.0 and 0.3 for primary, secondary and tertiary nitrates, respectively (Arey et al., 2001).

For β hydroxy peroxy radicals, α is divided by two to account for the effect of the hydroxy group as highlighted by O'Brien et al. (1998).

For acylnitrates, the yield is set to the alkyl tertiary nitrate yield, providing it does not exceed 4%.

3.2.2 NO_2

NO_2 reacts with peroxy acyl radicals to yield peroxyacylnitrate-like compounds, which decompose thermally or photolytically:

$$RC(O)OO + NO_2 \leftrightarrows RC(O)OONO_2 \quad \text{(R8)}$$

The rates of formation and decomposition of methyl peroxyacylnitrates (MPAN) are used for all PAN-like compounds except PAN itself. Most PAN-like compounds except PAN itself have other reactive groups (aldehyde, primary or a secondary alcohol, double bond) causing their major sink to be reaction with HO.

3.2.3 NO_3

NO_3 reacts with peroxy radicals through

$$NO_3 + RO_2 \rightarrow NO_2 + RO + O_2 \quad \text{(R9)}$$

The rate coefficient is set to 2.3×10^{-12} cm^3 molecule^{-1} s^{-1} independent of both the temperature and the peroxyradical.

3.2.4 HO_2 and peroxy radicals

HO_2 reacts with peroxy radicals through four different channels:

$$HO_2 + RO_2 \rightarrow ROOH + O_2 \quad \text{(R10)}$$

$$\rightarrow \mathrm{ROH} + \mathrm{O_3} \quad \text{(R11)}$$

$$\rightarrow \mathrm{RO} + \mathrm{HO} + \mathrm{O_2} \quad \text{(R12)}$$

$$\rightarrow \mathrm{R_{-H}O} + \mathrm{H_2O} + \mathrm{O_2} \quad \text{(R13)}$$

Reaction (R13) has only been observed for compounds such as $\mathrm{RCH_2OCH_2OO}$ and is not considered in this study. Acyl peroxides are assumed to react through Reaction (R10), Reaction (R11) and Reaction (R12) with a branching ratio 0.4:0.2:0.4 (Hasson et al., 2004; Jenkin et al., 2007). Acetonylperoxy radicals have also been shown to react through Reaction (R10) and Reaction (R12) with a branching ratio 1:2 (Hasson et al., 2004). The other alkylperoxy are assumed to react through Reaction (R10) only.

The reaction rate coefficient for the reaction of alkylperoxy with $\mathrm{HO_2}$ is set to $2.91\times10^{-13}\exp(1300/T)\times(1-\exp(-0.245n_c))$ $\mathrm{cm^3\,molecule^{-1}\,s^{-1}}$ where n_c is the number of carbon atoms (Saunders et al., 2003). For the acyl peroxy radicals, the reaction rate coefficient is set to $5.2\times10^{-13}\exp(983/T)$ $\mathrm{cm^3\,molecule^{-1}\,s^{-1}}$ based on the reaction of the methylacylperoxy.

$\mathrm{RO_2}+\mathrm{RO_2}$ reactions are neglected in this study. In the early stages of isoprene photooxidation the chemistry of peroxyradicals is entirely dominated by NO. At the end of the experiment, peroxy radical chemistry is dominated by $\mathrm{HO_2}$, which concentration is high enough so that $\mathrm{RO_2}$ + $\mathrm{RO_2}$ reactions can be safely neglected.

3.2.5 Photolysis

The photolysis rate of a compound i is computed via:

$$J_i = \int_{\lambda_1}^{\lambda_2} \mathcal{J}^e(\lambda)\sigma_i(\lambda)\,\phi_i(\lambda)\,d\lambda \quad (4)$$

The effective light flux $\mathcal{J}^e$ is computed using an experimental determination of J_{HONO} and a spectrum of the lamp output made every nanometer (LI-COR LI1800 λ_1=300 nm, λ_2=600 nm). σ_{HONO} is scaled using the oscillator strength recently reported by Wall et al. (2006).

The photolysis of compounds with unknown absorption cross sections is estimated from the known photolysis rate constants of similar compounds. The photolysis of organic nitrates is assumed to yield only RO + $\mathrm{NO_2}$. For primary organic nitrate, the photolysis rate is taken from $1\text{–}\mathrm{C_4H_9ONO_2}$, for secondary organic nitrates from $2\text{–}\mathrm{C_4H_9ONO_2}$ and for tertiary nitrates from tertbutylnitrate (Roberts and Fajer, 1989; Atkinson et al., 2006).

3.2.6 Fate of the alkoxy radicals

Alkoxy radicals can react following three different pathways:

$$\mathrm{R_1R_2R_3CO^{\cdot}} \rightarrow \mathrm{R_1R_2CO} + \mathrm{R_3^{\cdot}} \quad \text{(R14)}$$

$$+\mathrm{O_2} \rightarrow \mathrm{R_1R_2CO} + \mathrm{HO_2} \text{ if } \mathrm{R_3} = \mathrm{H} \quad \text{(R15)}$$

$$\rightarrow \mathrm{R_1R_2COHCCCC^{\cdot}R'_3} \quad \text{(R16)}$$

$$\text{with } \mathrm{R_3} = \mathrm{CCCCR'_3}$$

Since the isomerization reaction, Reaction (R16), requires at least four carbons (Atkinson, 1997), it occurs only at the very beginning of isoprene photooxidation, when major products retain five carbons. In the case of isoprene, isomerization (Reaction R16) is faster than decomposition (Reaction R14) and reaction with $\mathrm{O_2}$ (Reaction R15). Alkoxy radicals which cannot undergo Reaction (R16) are assumed to decompose through Reaction (R14), i.e. their reaction with $\mathrm{O_2}$ (Reaction R15) is generally neglected except for a few cases detailed in the discussion section.

Generally the decomposition of an alkoxy radical can occur through different channels, whose branching ratios (Y_i) are estimated using their respective activation energies, E_{bi}.

$$\mathrm{R_1R_2R_3CO^{\cdot}} \rightarrow \mathrm{R_2R_3CO} + \mathrm{R_1^{\cdot}} \quad \mathcal{Y}_1 \quad \text{(R17)}$$

$$\mathrm{R_1R_2R_3CO^{\cdot}} \rightarrow \mathrm{R_1R_3CO} + \mathrm{R_2^{\cdot}} \quad \mathcal{Y}_2 \quad \text{(R18)}$$

$$\mathrm{R_1R_2R_3CO^{\cdot}} \rightarrow \mathrm{R_1R_2CO} + \mathrm{R_3^{\cdot}} \quad \mathcal{Y}_3 \quad \text{(R19)}$$

with

$$\forall i \in (1,2,3)\ \gamma_i = \exp\left(\frac{E_{b1} + E_{b2} + E_{b3} - E_{bi}}{RT}\right) \quad (5)$$

E_b is calculated using the generalized structure-activity relationship developed by Peeters et al. (2004).

4 Isoprene mechanism considerations

4.1 Overview of the chemical evolution

The evolution of the chemistry in the chamber can be summarized by two different proxies: the overall speciation (Fig. 1) and the chemical speed defined as $\nu = \frac{d[CO+CO_2]}{dt}$ (Fig. 2). Both feature three different regimes:

First regime (0 <t< 150 min). This regime is characterized by a large supply of NO, as well as very reactive compounds featuring a double bond. ν reaches a maximum after a few minutes at 0.7 ppC/min. O_3 and PNA are very low in this regime, underlying a chemistry dominated by NO. The organic nitrate concentration reaches its maximum at the end of this regime. The reduction in [HO] corresponds to an increase of [NO_2] leading to the formation of nitric acid.

Second regime 150<t<550 min. This regime is characterized by a very stable ν (0.5 ppbv(C)/min) with a chemistry dominated by aldehydes. HO recycling though HO_2 + NO is less efficient than in the first regime due to the abundance of O_3 which favors the formation of PAN. Nevertheless the reduction in the chemical speed due to the transition from "double bond dominated" to "aldehyde dominated" reduces HO sinks which ultimately leads to a slow increase in HO, leveling off when PNA peaks, i.e. when the NO_X is titrated.

Third regime 550<t<1000 min. After the PNA peak, the chemistry is dominated by HO_2, as evidenced by the formation of peracetic acid (CF_3O^- cluster at m/z=161) and methylperoxide (CF_3O^- cluster at m/z=133). Low-reactivity compounds such as ketones or long-lived nitrates dominate the chamber composition. Despite the almost constant HO, the chemical speed drops significantly to 0.1 ppbv(C)/min.

In order to limit the uncertainties (cf. Appendix C), the further discussion is focused on the NO_X dominated regime, i.e. regimes 1 and 2.

4.2 Isoprene branching ratio and isoprene nitrate yield constraints

Under chamber experimental conditions, isoprene photooxidation proceeds mainly through the addition of HO to the two double bonds (positions 1, 2, 3 and 4, cf. Fig. 3). Additions to positions 1 and 4 can be followed by resonance, giving rise, after addition of O_2, to four resonance peroxy radicals (Sprengnether et al., 2002), referred to as Z/E (1,4) and Z/E (4,1). The reported branching ratios for these eight peroxy radicals widely vary (Lei et al., 2001). In the following we will denote the different channels by the couple (i,j), where i and j refer, respectively, to the carbon on which the HO and O_2 addition occurs.

The isoprene peroxy radicals react almost exclusively with NO to form either alkoxy radicals or organic nitrates (Reaction R7). For simplicity we assume that the nitrate yields from the isoprene peroxy radicals formed in the non-resonance channels, α_{nr}, ((1,2), (2,1), (4,3) and (3,4)) are identical. MACR is only produced through the reaction of the alkoxy radicals originating from channels (1,2) and (2,1) with NO and by ozonolysis of isoprene. Since the latter accounts for less than 0.5% of the total isoprene consumption in the chamber, we can use the experimental MACR yield (Sprengnether et al., 2002; Karl et al., 2006) to constrain α_{nr} and the branching ratio (Y) of channels (1,2) and (2,1).

$$(1 - \alpha_{nr})(Y_{1,2} + Y_{2,1}) = 0.41 \quad (6)$$

In a similar fashion we constrain the branching ratios of the channels (4,3) and (3,4) using the experimental yield of MVK (Sprengnether et al., 2002; Karl et al., 2006):

$$(1 - \alpha_{nr})(Y_{4,3} + Y_{3,4}) = 0.27 \quad (7)$$

Lei et al.'s theoretical study (2001) provides additional constraints on the HO addition at positions 1,2,3, and 4:

$$Y_{1,2} + Y_{1,4} = 0.56 \quad (8)$$

$$Y_{4,3} + Y_{4,1} = 0.37 \quad (9)$$

$$Y_{2,1} = 0.020 \quad (10)$$

$$Y_{3,4} = 0.050 \quad (11)$$

As shown in Sect. 4.4.1, the decomposition isoprene nitrate formed in the (4,1) branch, ISOPN (4,1), yields propanone nitrate (PROPN_N) and dihydroxybutanone (DHB), which are both detected by CIMS. The former is a long-lived compound observed at m/z=204 with a molar yield of about 1%. The latter, measured at m/z=189, has a molar yield of 2.8%. Assuming ISOPN(4,1) decomposition is the sole source of DHB, while PROPN_N is yielded from the decomposition of both ISOPN(4,1) and ISOPN(2,1):

$$(1 - \alpha_{2,1}^{dn})\gamma\alpha_{nr}Y_{2,1} + (1 - \alpha_{4,1}^{dn})\alpha_r Y_{4,1} = 0.038 \quad (12)$$

where α_r is the nitrate yield for ISOPN (4,1), γ is the branching ratio of the pathway yielding propanone nitrate from ISOPN(2,1), computed using (5), $\alpha_{2,1}^{dn}$ and $\alpha_{4,1}^{dn}$, the respective organic dinitrate branching ratios from ISOPN(2,1) and ISOPN(4,1). To proceed, we assume that the yield of ISOPN (1,4) is identical to the yield of ISOPN (4,1).

Noting that the use of the Eqs. (6) to (12) to solve for α_{nr}, α_r and $Y_{i,j}$ does not yield a single solution, we use the branching ratios derived by Lei et al. (2001) to initialize the numerical solution of this non-linear system and obtain: $Y_{1,2}$=0.4075, $Y_{1,4}$=0.1525, $Y_{2,1}$=0.02, $Y_{4,3}$=0.2315, $Y_{4,1}$=0.1385, $Y_{3,4}$=0.05, α_r=0.257, α_{nr}=0.0409.

Noteworthy is the much higher nitrate yield for the resonance branches (α_r) than for the non-resonance branches (α_{nr}). This conclusion bears a striking similarity with the estimate derived by Giacopelli et al. (2005) using a corrected Carter's parameterization.

We can use the isoprene nitrates profiles to assess the accuracy of these estimates (cf. Sect. 4.4.1). The yields appear to be underevaluated due to ISOPN(1,2)

and ISOPN(4,3). Reducing the yields of MVK and MACR by one percentage point greatly improves the simulation of the isoprene nitrates. These yields are well within the uncertainties of both the studies we use (Sprengnether et al., 2002; Karl et al., 2006).

Therefore, we use the following modified parameters: $Y_{1,2}$=0.404, $Y_{1,4}$=0.156, $Y_{2,1}$=0.02, $Y_{4,3}$=0.226, $Y_{4,1}$=0.144, $Y_{3,4}$=0.05, α_r=0.241, α_{nr}=0.057.

4.3 Resonance channels

Although many studies have focused on the main decomposition channels yielding MACR and MVK (Paulson et al., 1992; Sprengnether et al., 2002; Karl et al., 2006), the resonance channels ($Z_{1,4}$, $E_{1,4}$, $Z_{4,1}$, $E_{4,1}$) remain poorly constrained. This is a major weakness, as these pathways account for more than 30% of the carbon and a large fraction of the nitrates.

4.3.1 (1,4) branch

Here we describe the mechanisms relevant to the (1,4) branch (Fig. 4).

$Z_{1,4}$. After its reaction with NO, the peroxyradical undergoes a δ_1^5 isomerization (R16). If the isomerization is immediately followed by a resonance, the decomposition of the alkoxy radical yields methylpropanedial (MPDL). The alkoxy radical can also undergo a suite of reactions described by Dibble (2004a,b) which ultimately leads to the formation of glycolaldehyde and methylglyoxal, referred to as GLYC and MGLYX. This reaction, reproduced below, is based on the stabilization of the alkoxyradical through a double H bond which prevents its decomposition while enhancing a δ_5^1 shift with the H of the alcohol group.

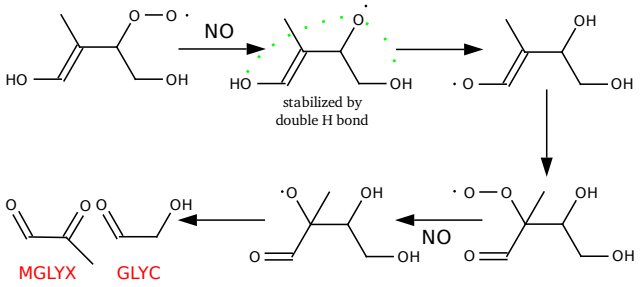

If the isomerization is not followed by resonance, reaction with O_2 leads to the formation of (2Z)-4-hydroxy-2-methylbut-2-enal, referred to as HC5Z(1, 4), measured as a cluster at m/z=185 (Fig. 5). The detection of its ^{13}C isotope at m/z=186 supports the attribution of the signal to HC5.

The 3-methylfuran (3-MF) formation mechanism proposed by Francisco-Marquez et al. (2005) is implemented in the model for the two cis channels ($Z_{1,4}$ and $Z_{4,1}$).

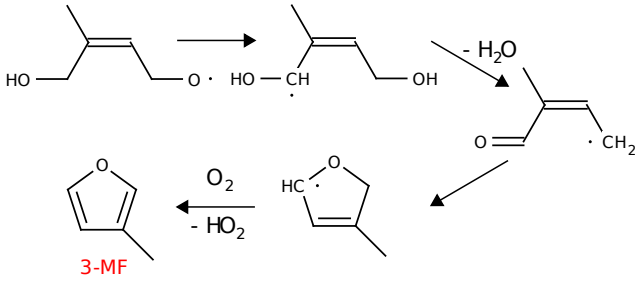

Regarding the HC5 Z(1,4) fate, HO can add to the double bond (Fig. 4, channels 2 and 3), abstract the aldehydic H (channel 4) or the H in α of the alcohol (channel 1). The preferred

addition on the double bond is expected to yield glycolaldehyde and methylglyoxal. The signal detected at mass m/z=217 (Fig. 6) is attributed to 2,4-dihydroxy-2-methyl-3-oxobutanal (DHMOB (1,4)) originating from channel 3: if the alkoxy radical formed after addition of HO on the less preferred location is stabilized by a double H bond, slowing unimolecular decomposition, it may react with O_2 to yield DHMOB (1,4). Channel 4 leads to the formation of a 5 carbon acid: (Z)-2-methyl-4-oxobut-2-enoic acid (MOBA Z(1,4)). The similarity (ρ=0.93 for the first 400 min) of the signal detected at m/z=199 (CF_3O^- cluster) and m/z=133 (F^- transfer) highlights the acidic character of the detected compound and supports the attribution of these signals to MOBA (Fig. 7).

$E_{1,4}$. The first isomerization can be followed by resonance to yield 2-(hydroxymethyl)prop-2-enal (HMPL). A second isomerization would yield 4-hydroxy-3-oxobutanal (HOBL) if followed by resonance or 4-hydroxy-3-(hydroxymethyl)but-2-enal (MHBL). The further photooxidation of HMPL and MHBL yield mainly dihydroxypropanone (DHPN), whose CF_3O^- cluster is observed at m/z=175 (Fig. 8), and hydroxyoxopropanal (HOPL) whose cluster is observed at m/z=173 (Fig. 9). The reaction of HO with the latter can form an acylperoxy which can further react with NO_2 yielding a PAN-like compound, 3-hydroxy-oxo-peroxyacylnitrate (cluster at m/z=250), referred to as PAN 250 (cf. Sect. 4.6).

4.3.2 (4,1) branch

Since the relevant mechanisms for the (4,1) pathway (Fig. 10) are closely related to those of the (1,4) branch, we only describe the differences

$Z_{4,1}$. Applying the Dibble mechanism to the resonance branch results in the formation of hydroxyacetone and glyoxal, referred to as HACET and GLYX. The addition of HO to the less preferred position of HC5(4, 1)Z (and (4, 1)E) leads to the formation of 3,4-dihydroxy-3-methyl-2-oxobutanal referred to as DHMOB (4,1) (Fig. 6).

$E_{4,1}$. The alkoxy radical configuration prevents δ_1^5 isomerization (R16) as well as decomposition (R14) from occurring. Therefore it is expected to react entirely with O_2 (R15) to yield a HC5 isomer (HC5 (4,1)E).

4.3.3 Channel asymmetry

Because the CIMS observations can trace carbon flow through the (1,4) branch, they provide valuable insight into the partitioning between the cis and trans channels.

The branching ratio between the non resonance (Y_{nr}) and the resonance (Y_r) channels is set to Y_{nr}=62% and Y_r=38%, based on the branching ratio between (4,1) and (4,3). In E_1, HOPL does not feature an early source (Fig. 9), indicating that the resonance channel yielding HMPL is negligible. Indeed, its formation appears unfavorable on both a thermodynamic (the double bond is less substituted) and a kinetic (formation of a secondary radical) basis. Thus, the branching ratio is set to $Y_{nr}^{E_{(1,4)}}$=95% and $Y_r^{E_{(1,4)}}$=5%.

The $E_{1,4}$ chemistry is different from the other branches as it does not yield an HC5 isomer. The major products of this channel are also all observed: HOPL, DHPN, and HOBL. This specificity allows us to constrain the branching ratio between the cis and the trans peroxyradical of the (1,4) branch. If an equal partitioning of the carbon is assumed between $E_{1,4}$ and $Z_{1,4}$, the concentrations of both HOPL and DHPN are largely overestimated while the concentration of HC5=HC5 (1,4)Z+HC5 (4,1)E+HC5 (4,1)Z is underestimated. The best agreement is obtained when,

$$\frac{Y_{E_1}}{Y_{Z_1}} = \frac{3}{17} \tag{13}$$

In addition, no significant 3-methylhydroxy-4-hydroxy-butenal (MHBL) is observed (cluster at m/z=201) despite its structural similarity with HC5, suggesting that little flux of carbon occurs through $E_{1,4}$. We use k_{HO}=6.13×10^{-12} cm^3 molecule^{-1} s^{-1} for DHPN (25% more than the SAR estimate) and k_{HO}=2.23×10^{-11} cm^3 molecule^{-1} s^{-1} for HOPL in order to capture properly their measured profiles (Figs. 8, 9). Note that the signal at m/z=173 also includes pyruvic acid whose chemistry is described in Sect. 4.5.

The asymmetry between Z/E isomers contradicts the conclusions drawn from quantum mechanical calculations (Dibble, 2002) as well as the assumption made by most

kinetic models of isoprene photooxidation (Paulson et al., 1992; Fan and Zhang, 2004).

The discrepancy with quantum mechanical calculations may be related to a difference in the reaction of the cis/trans radical with O_2. The radicals are formed with approximately 40 kcal/mol excess energy. The minimum isomerization barrier is estimated to be about 15 kcals/mol (Dibble, 2002). Therefore, assuming a collision stabilization of 100 cm^{-1}collision^{-1}, the radicals undergo nearly 100 collisions (20 with O_2) before they are cooled below the isomerization barrier. If, based on reported rate coefficients for R$^\bullet$+O_2 (Atkinson et al., 2006), one reaction among ten is assumed to be reactive, peroxyradicals are likely to be formed before the isomers are cooled below the isomerization barrier. Therefore, the equilibrium may be shifted if the reaction of the trans radical with O_2 is faster than the reaction of the cis radical. Measurements made with reduced partial pressure of O_2 could test this hypothesis.

The molar yield of 3-methylfuran (3MF) is set to 4.5% based on experimental results (Atkinson et al., 1989; Paulson et al., 1992). With the yields we derived from constraints (6) to (13), 37% of the peroxyradical formed in the $Z_{1,4}$ and $Z_{4,1}$ branches must decompose to 3MF. Since 3-methylfuran requires the parent peroxy radical to be cis, if the branching ratio E/Z were close to 1:1, it would require the fraction of peroxy radical $Z_{1,4}$ and $Z_{4,1}$ decomposing to 3-methylfuran to be 62%, which would lead to a molar yield of HC5 of 6.1%, more than 30% lower than the derived yield (Table 2).

The fast decay of HC5 (Fig. 5) requires a very fast reaction rate with HO: 1.2×10^{-10} cm^3 molecule^{-1} s^{-1} . This estimate is consistent with the fastest rate recently derived by Baker et al. (2005) and about 80% greater than the SAR estimate (k_{HO}^{SAR}=6.82×10^{-11} cm^3 molecule^{-1} s^{-1} or 7.9×10^{-11} cm^3 molecule^{-1} s^{-1} with the correction from Bethel et al., 2001; Papagni et al., 2001). We do not find any evidence for a longer lived HC5. From the yield of MOBA=MOBA Z(1,4)+MOBA Z(4,1) (Fig. 7 and Table 2), we derive a branching ratio of about 25% for channel 4, consistent with that inferred from Kwok's SAR. Therefore, we increase the rates of channels 2,3 and 4 by 80% in order to match the observed decay of HC5. Papagni et al. (2001) have shown that an alcohol group in α of a double bond enhances the addition of HO to the double

bond, which may explain some of the discrepancy observed for channels 2 and 3. The discrepancy regarding channel 4 may be related to a long distance interaction between the alcohol group and the carbonyl group (Neeb, 2000).

Setting the branching ratio channel ②:③ to 2/3 and $k_{HO}=1\times10^{-11}$ cm^3 molecule^{-1} s^{-1} captures the profile of DHMOB=DHMOB(1,4)+DHMOB(4,1) (Fig. 6).

4.3.4 Evidence for Dibble's mechanism

Both hydroxyacetone (Fig. 11) and glycolaldehyde (Fig. 12) profiles exhibit a very prompt source in the chamber. To our knowledge, the mechanism proposed by Dibble (2004a,b) and reproduced in Sect. 4.3.1 is the only mechanism able to yield both compounds from isoprene in one step, i.e. following the first HO addition on isoprene. The best agreement is found if an equal partitioning between the straight decomposition and Dibble's mechanism is assumed. The hydroxyacetone rate constant with HO is set to $k_{HO}=5.98\times10^{-12}$ cm^3 molecule^{-1} s^{-1} (Dillon et al., 2006) and the rate constant of glycolaldehyde with HO was set to $k_{HO}=8\times10^{-12}$ cm^3 molecule^{-1} s^{-1} (Karunanandan et al., 2007).

4.4 Organic nitrates

The formation of organic nitrates, and more specifically isoprene nitrates, play an important role in determining the amount of NO_x and thus ozone production in many environments. The observation of isoprene nitrate clusters with CF_3O^- as well as some of the products of their photooxidation, provides constraints on the isoprene nitrate yields, the amount of NO_x recycled through the first stage of their photooxidation, and their lifetimes. These three parameters are necessary to accurately assess the influence of isoprene nitrates on atmospheric chemistry.

Yield. Previous estimates for the isoprene nitrate yield, α, span a very large range. Chen et al. (1998) reported a global yield of 4.4%, Chuong and Stevens (2002), 15% using an indirect

method, Sprengnether et al. (2002), 12%, Patchen et al. (2007), 7% at 130 hPa. Giacopelli et al. (2005) proposed to use Arey et al. (2001)'s nitrate estimate with O'Brien et al. (1998)'s correction for the β-hydroxynitrates ((1,2);(2,1);(3,4);(4,3)) and Espada and Shepson (2005) correction for (1,4) and (4,1) isoprene nitrates, and report a yield of 5.5% for the former and 15% for the latter, for a global yield of 8.6%. Since organic nitrates sequester NO_x, such a large variation in the estimated yields has profound implications in the assessments of ozone production caused by isoprene photooxidation (von Kuhlmann et al., 2004; Fiore et al., 2005; Horowitz et al., 2007).

Recycling. The efficiency of the NO_x sequestration depends on the fate of the isoprene nitrates and especially on how much NO_x is released in their subsequent photooxidation. Horowitz et al. (2007) obtain the best agreement with the boundary layer data when 40% of the NO_x is recycled with a low nitrate yield (4%).

Lifetime. The efficiency of both NO_x transport and removal through organic nitrates is related to their lifetimes. The transport of isoprene-nitrates and further alkylnitrates is of special importance since it is thought to be a major source of NO_x in rural areas (Horowitz et al., 1998). In this NO_x-limited environment, these nitrates constitute one of the main factors determining O_3 production. In the absence of experimental data, their lifetime was estimated by Giacopelli et al. (2005) using Kwok's SAR.

NO_x-recycling is defined as the difference between the NO_x released by the reaction and the NO consumed. As a result, since ISOPN(2, 1) oxidation does not yield any NO_2, its recycling is negative due to the formation of dinitrates (Fig. 13 and Table 1), which have been observed at m/z=311.

4.4.1 ISOPN (1,4) and (4,1)

The fate of the isoprene nitrates originating from the resonance channels (1,4) and (4,1), respectively ISOPN (1,4) and ISOPN (4,1), can be followed using ethanal nitrate (ETHL_N) monitored at m/z=190 (Fig. 15) and propanone nitrate (PROPN_N) at m/z=204 (Fig. 16). Both compounds appear earlier than MACR nitrate (MACR_N) and MVK nitrate (MVK_N), which are formed from both their parent alkenes and the de-

composition of the non-resonance isoprene nitrates (ISOPN 1,2 and ISOPN 4,3). Both MACR_N and MVK_N are monitored at m/z=234 (Fig. 18). The early appearance of ETHL_N and PROPN_N requires that their parent nitrates react much faster with HO than the non-resonance isoprene nitrates.

Using PROPN_N as a proxy to infer the reaction rate of ISOPN (4,1) with HO, we find $k_{HO}^{ISOPN(4,1)}=8.5\times10^{-11}$ cm^3 molecule^{-1} s^{-1} , about 30% faster than the SAR estimate. This discrepancy may be related to the inadequate parameterization of the effects of nitroxy groups (Neeb, 2000) on the reactivity of the double bond. No significant signal is observed at m/z=230, confirming that the abstraction of the hydrogen in α of the alcohol is negligible.

Using PROPN_N and DHB, we estimate the NO_x recycling from the (4,1) branch to be about 70%. The reaction rate coefficient of DHB with HO is estimated to be 1.3×10^{-11} cm^3 molecule^{-1} s^{-1} or 60% of SAR (Fig. 17).

SAR predicts that $k^{ISOPN(4,1)}=k^{ISOPN(1,4)}$. Indeed, ETHL_N features an early source (Fig. 15), which suggests a fast decomposition of its parent nitrate ISOPN (1,4) (Fig. 13). The use of the primary nitrate photolysis rate (cf. 3.2.5) and SAR rate estimate for the reaction ETHL_N + HO underpredicts its decay. ETHL_N was monitored in a similar experiment featuring a lower HO concentration and its lifetime was slightly longer suggesting that this discrepancy originates from a faster HO sink rather than from an error in the photolysis rate. To match the measured profile (Fig. 15), we take $k_{HO} = 1\times10^{-11}$ cm^3 molecule^{-1} s^{-1} , three times faster than the SAR estimate. The formation of formic acid from the ISOPN (1,4) branch is discussed in Sect. 4.5.

NO_x recycling from ISOPN (1,4), 52%, is slightly less than that predicted for (4,1) due to the formation of a minor MVK_N(m) (Fig. 13) as explained in further details in Sect. 4.4.3.

4.4.2 ISOPN (1,2) and (4,3)

The fate of ISOPN (1,2), ISOPN (4,3) is more difficult to constrain since the products of their decomposition have multiple sources. Therefore, SAR is used to constrain the ratio of their rates constants. The absolute rate coefficients were reduced by 20% from SAR to match the measured profile (Table 1).

To constrain NO_x-recycling, we assume that the branching ratio toward glycolaldehyde and hydroxyacetone is identical in the decomposition of ISOPN (1,2) and ISOPN (4,3). MACR_N and MVK_N require a large isoprene nitrate source to match their observed profiles (Fig. 18); we find an optimal branching ratio of 0.3 for the NO_x recycling channel.

The reaction of the isoprene nitrate with ozone is included for ISOPN (1,2) and ISOPN (4,3), because their long lifetimes allow them to encounter high concentrations of ozone in the chamber (Fig. 2). We do not observe the formation of 3 hydroxy-2-nitrooxy-2-methyl propanoic acid (no correlation between m/z=184 and m/z=250). Therefore, we use a simplified version of the products proposed by Giacopelli et al. (2005) assuming that this reaction yields only MACR_N and MVK_N, constituting the late source of MVK_N (Fig. 18). Note that isoprene nitrate ozonolysis represents a significant source of MACR_N (Table 2) in the mechanism.

4.4.3 Methacrolein and methylvinylketone nitrates

MVK_N and MACR_N are monitored through their clusters with CF_3O^- at m/z=234 (Fig. 18).

The abstraction of the hydrogen in α of the alcohol in MACR_N , MVK_N and MVK_N (m) is expected to yield dicarbonyl nitrates. Their structural similarity with PROPN_N as well as their significant dipole moments suggests that the CIMS should sensitively detect these compounds at m/z=232. Since this signal does not feature any significant product except isoprene nitrates, another decomposition mechanism is hypothesized. In Sect. 4.4.1, we assumed that the α-hydroxy-alkylperoxy radicals originating from

ISOPN (1,4) could yield formic acid. Applying a similar mechanism to MVK_N and MVK_N (m) yields formic and pyruvic acid respectively. In contrast to ISOPN (1,4), the level of NO is low while MVK_N and MVK_N(m) react, and so, this mechanism may operate through an intramolecular decomposition rather than reaction with NO. Such a reaction may involve a four or six-e$^-$ mechanism.

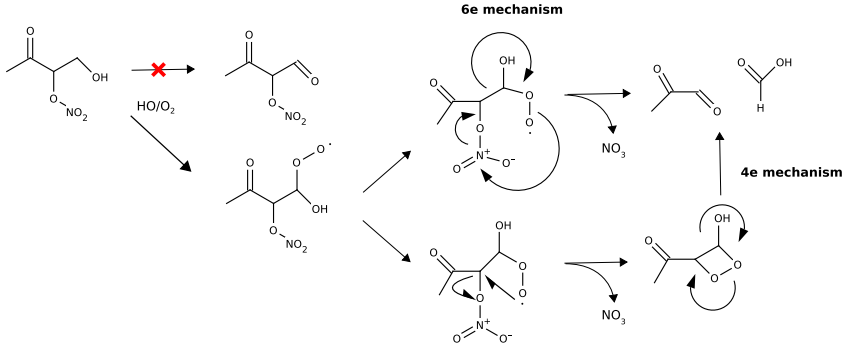

The absence of a second peak at m/z=232 also suggests that the abstraction of the aldehydic H dominates over the abstraction of the H in α of the alcohol for MACR_N. This reaction leads to the formation of hydroxyacetone. It also suggests that MACR_N has a much shorter lifetime than MVK_N, consistent with the recorded profile which features an early peak followed by a slow decay (Fig. 18). Nevertheless, the reaction of MVK and MACR with HO is too slow to account for the steep rise of the signal in the first few dozen minutes, highlighting the importance of the formation of MVK_N (m) from the highly reactive ISOPN (1,4) (Fig. 13).

Using k_{HO}^{MVK}=1.47×10^{-11} cm^3 molecule^{-1} s^{-1} (Karl et al., 2006), we derive a nitrate yield, α_{MVK}, from MVK using the glycolaldehyde profile (Fig. 12) of α_{MVK}=10%. This value is consistent with the study of Chuong and Stevens (2004). Using the tail of the m/z=234 signal, we derive the reaction rate coefficient of MVK_N

with HO: k_{HO}^{MVKN}=2.8×10^{-12} cm^3 molecule^{-1} s^{-1} . Applying the same approach to MACR/MACR_N/HACET is more complicated since hydroxyacetone has many more sources than glycolaldehyde (Fig. 11 and Table 2). We set the yield of MACR_N to 15% and its reaction rate coefficient with HO to 5×10^{-11} cm^3 molecule^{-1} s^{-1} in order to match the peak time of m/z=234. Finally capturing the early source of m/z=234 requires the yield of MVK_N(m) from ISOPN (1,4) to be about 15%.

4.4.4 Fate of organic nitrogen

The large difference in the yields and fate of the nitrates formed in the resonance and non-resonance channels may explain some of the differences in the yields and NO_x recyclings reported in the literature. Despite their formidable yield, the resonance isoprene nitrates have a limited effect on the NO_x budget due to their short lifetime and high NO_x recycling. In contrast, the peroxy radicals originating from the non resonance channels are less prone to form organic nitrates, but the decomposition of these organic nitrates is slow and releases little NO_x. This is consistent with the study of Horowitz et al. (2007) which suggested a similar NO_x recycling despite a much smaller isoprene nitrate yield. The large spread of reported isoprene yields may also be attributed to the lifetime difference between the resonance and non-resonance channels. Studies focusing on the very first step of isoprene photooxidation (Sprengnether et al., 2002) tend to report the highest nitrate yield, since they are able to monitor this class of isoprene nitrates, see inset of (Fig. 14). The same argument may explain the observations of a greater variety of isoprene nitrates in laboratory experiments than in the field (Giacopelli et al., 2005).

Propanone nitrate, and to a lesser extent MVK_N, are long-lived organic nitrates, which make them suitable to transport NO_x to rural regions or to be a significant NO_x sink through deposition. Both MACR_N and MVK_N appear to release NO_x in the course of their decomposition, possibly through the formation of formic and pyruvic acids.

Finally, despite the large recycling at every step of the mechanism, the amount of organic nitrates in the system decreases very slowly over the course of the experiment (Fig. 2) due to the formation of long-lived nitrates.

4.5 Acids

Small carboxilic acids are ubiquitous in the atmosphere both in the gas-phase and in the aqueous phase (Chebbi and Carlier, 1996). In these experiments, very high yields of these acids were observed.

4.5.1 Formic acid

In these studies, formic acid is detected as a cluster (m/z=131) and a transfer (m/z=65) with about equal sensitivity. At the NO_x titration, a molar yield of about 10±2% is obtained (Fig. 20).

The measured profile of formic acid (Fig. 20) features the three characteristic chemical regimes of this experiment as described in Sect. 4.1:

First regime. A very early source of formic acid is noticeable (Fig. 20). This source is absent from the experiments performed in the absence of NO_x. As mentioned in 4.4, we believe that this source arises from the decomposition of ISOPN (1,4) and ISOPN (3,4) (Fig. 13): the stabilization of the primary [1-hydroxy-2-(nitrooxy)ethyl]peroxy radical (Hermans et al., 2005) may be sufficiently enhanced by the nitroxy group so that its intramolecular decomposition (or the formation of the alkoxy radical through its reaction with NO) can compete with the straight conversion into ethanal nitrate. Furthermore, a complete decomposition of ISOPN (1,4) into ETHL_N would largely overpredict its measured profile suggesting another decomposition pathway. Matching the ETHL_N profile (Fig. 15) results in a branching ratio formic acid to ETHL_N of 3:1. ISOPN(2, 1) may yield acetic acid, but is not included since its contribution would be negligible. In addition, secondary α-hydroxy-alkylperoxy radicals have been shown to be less stable than primary ones (Hermans et al., 2005).

Bierbach et al. (1995) report 4-oxo-pentenal as the major product of the photooxidation of 2-methylfuran in the absence of NO_x, while formic acid accounts for about 6%. We are unaware

of any study of the photooxidation of 3-MF in the presence of NO_x. Since the reaction rate of methylfuran with HO is similar to that derived for ISOPN (1,4) and (4,1), its photooxidation may contribute to the early sources of formic acid.

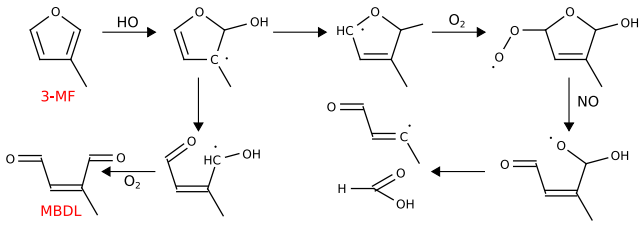

Second regime. Butkovskaya et al. (2006a,b) report a formic acid yield from the photooxidation of glycolaldehyde (hydroxyacetone) of 18% (respectively 7%). The formation of formic acid from the decomposition of MVK_N described in 4.4.3 also plays a minor role in this regime.

Third regime (not shown). As NO_x becomes limiting, hydroxymethyl hydroperoxide (HMHP) becomes the main source of formic acid through its reaction with HO or its photolysis. Its main formation channel is the ozonolysis of MVK/MACR which yields CH_2OO which subsequently forms HMHP after reacting with water (Ryzhkov et al., 2004). We note that a large additional source is missing in the mechanism. Although gas-phase processes cannot be ruled out to explain this continuous increase of formic acid, they are unlikely to be its main cause. Indeed, most VOC have already been oxidized into carbon monoxide or carbon dioxide at this point. This phenomenon may be related to aerosol processes (Walser et al., 2007). The decrease of the aerosol volume in this stage of the photooxidation can be estimated at $-2.5\ \mu m^3/cm^3$ which would represent a release of 2.6 ppbv "CO" in the chamber assuming a density of 1.25 g/cm^3 (Kroll et al., 2006). Since the same phenomenon is observed for acetic acid (Fig. 19), most likely both HO_x-dominated VOC oxidation as well as organic aerosol oxidation are needed to explain the observed increase in formic and acetic acid in the third regime.

4.5.2 Acetic acid

The production of acetic acid (Fig. 19) occurs primarily through the oxidation of hydroxyacetone as described by Butkovskaya et al. (2006b). Additional routes include direct formation from CH_3CHO + HO (Cameron et al., 2002) as well as $CH_3C(O)OO$ + HO_2 following reaction Reaction (R11).

Two additional routes are hypothesized: 1) decomposition of MACR_N(m), 2) decomposition of DHMOB (1,4) (m/z=217), inspired by the mechanism proposed by Butkovskaya et al. (2006a). Following their analysis, we assume a 37% acetic molar yield, the remaining falling apart as CO_2 and hydroxybutane-2,3-dione (m/z=187).

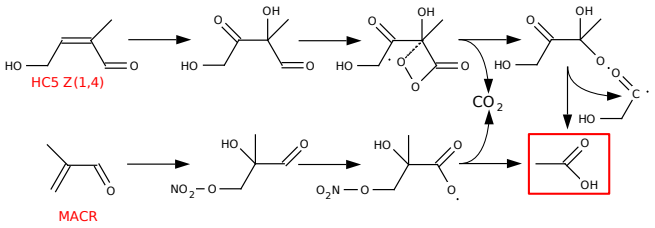

Note that acetic and formic acids are highly correlated after the first 150 min (ρ=0.988), since their main source, hydroxyacetone for acetic acid and glycolaldehyde for formic acid, share a similar origin (Table 2 and Figs. 19 and 20). We find [Acetic Acid]=0.46 ± 0.02 × [Formic Acid] − 0.92 ± 0.45. Such a strong correlation has been observed previously over Amazonia (Andreae et al., 1988) and Virginia (Talbot et al., 1995). Despite different conditions, the main source of both acids in the chamber is unlikely to result from the ozonolysis of the alkenes but rather originates from hydroxyacetone and glycolaldehyde, possibly accounting for part of the discrepancy between models (Jacob and Wofsy, 1988) and atmospheric observations (Andreae et al., 1988; Talbot et al., 1990).

4.5.3 Pyruvic acid

Pyruvic acid is a precursor for glyoxylic and oxalic acids, two carboxylic acids detected in the aerosol phase (Carlton et al., 2006). Pyruvic acid is observed at m/z=173 in addition to HOPL (Fig. 9). About 15% originates from the hydrolysis of the Criegee intermediate produced in the ozonolysis of MACR. Its main source in the chamber is the decomposition of MVK_N(m) following the scheme presented in Sect. 4.4.3.

In Fig. 9, the concentration of pyruvic acid appears to be overevaluated in the model by a factor of two. Even though the mechanism remains uncertain, the yield of MVK_N (m) is constrained by numerous proxies including glycolaldehyde, MVK_N/MACR_N and ISOPN(1, 4). Furthermore, no experimental calibration could be derived for this compound due to its stickiness to the walls of the flow tube, which suggests that the concentration of pyruvic could be underevaluated using the calibration derived from the thermal collision rate approach.

4.5.4 MOBA

The 5 carbon acids introduced in Sect. 4.3 can react with HO and ozone under the chamber conditions. Assuming HO reacts entirely at the double bond, the acid group would have to significantly reduce the rate coefficient of the HO addition in order to explain the long lifetime of this compound (Fig. 7). k_{HO} is set to 3×10^{-12} cm^3 molecule^{-1} s^{-1} , which corresponds to F_{COOH}=0.1 in terms of SAR and k_{O_3}=2×10^{-17} cm^3 molecule^{-1} s^{-1} . Furthermore the absence of detection of oxoacetic acid suggests that the HO addition on the double bond occurs on β of the acid group. Ozone appears to be the main sink of MOBA in this experiment due to the high ozone concentrations reached in the chamber.

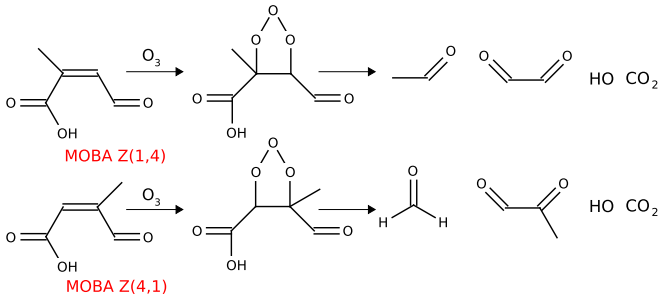

4.6 Open questions

In the previous sections, we have shed light on some of the complexity involved in understanding the photooxidation mechanism of isoprene. Additional work remains to be done, as illustrated by our inability to explain the signals observed at several m/z:

m/z=149. A significant signal is observed at m/z=149 very early in the experiment. HMHP cluster is expected to be observed at this m/z but should not be formed in significant amounts until the end of the second regime, when the peroxy radical chemistry begins to be dominated by HO_2. This early signal may be attributed to (2Z)-2-methylbut-2-enedioic acid (transfer) which has been shown to be produced from methyl maleic anhydride + water as illustrated below:

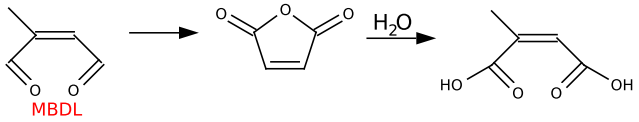

Nevertheless, if the attribution is correct, this compound would need a more direct pathway.

m/z=194. A significant signal is observed which may be attributed to the PAN-like compound $HOCH_2OONO_2$. Reported equilibrium data however preclude it from being present in substan-

tial amounts (Barnes et al., 1985); capturing the measured intensity would require an equilibrium constant close to that of HO_2NO_2. Another candidate is $HOOCH_2ONO_2$, which could originate from:

$$RCO - CH_2ONO_2 \longrightarrow CH_2ONO_2 \quad \text{(R20)}$$

$$CH_2ONO_2 \xrightarrow{O_2} OOCH_2ONO_2 \quad \text{(R21)}$$

$$OOCH_2ONO_2 \xrightarrow{HO_2} HOOCH_2ONO_2 \quad \text{(R22)}$$

Nevertheless, one would not expect any substantial formation via this mechanism in the NO_x dominated regime.

m/z=250. In Fig. 3, we depict the possible formation of a PAN like compound, which could account for the signal observed at m/z=250. The reaction of HO with oxyhydroxypropanone is expected to proceed mostly through the abstraction of the aldehydic H. The peroxy radical can then react with NO_2 to yield a pan-like compound which is observed at m/z=250. The peroxy radical can react with NO_2 to yield a pan-like compound which may be observed at m/z=250.

Another candidate is 3-hydroxy-2-nitrooxy-2-methyl propanoic acid, an acid that may form in the ozonolyzis of ISOPN(1,4) (Giacopelli et al., 2005). Nevertheless no F^- transfer to this acid at m/z=179 is observed.

5 Atmospheric relevance and reduced mechanism

A substantial fraction of the terrestrial Northern Hemisphere is characterized by conditions in which the fate of isoprene peroxy radical is dominated by reaction with NO The mechanisms derived in this study are, therefore, relevant for atmospheric chemical transport modeling. Of particular interest is the importance of propanone nitrate and MVK nitrate for the global NO_x budget in general and NO_x transport in particular. We also show that the photooxidation of organic nitrate may provide a large additional source of small carboxilic acids in the environment.

The full chemical mechanism described in this study is too large to be included in most atmospheric chemistry simulations. To aid in such investigations, we have derived a reduced mechanism that attempts to minimize the complexity while providing a description of the rich chemistry of the resonance channels (Table 3). This reduced mechanism 1) maintains carbon and nitrogen balance and 2) accurately describes the chemical ratio and product yields. The reduced mechanism includes several aspects of the isoprene oxidation that have been elucidated in this investigation and which are not adequately described in the isoprene oxidation mechanisms currently in chemical transport models (e.g. MOZART Pfister et al., 2008). These include an improved description of the resonance peroxy channels (that account for more than one-third of the carbon flux and a large fraction of the nitrate yield) and the formation of long-lived nitrates and carboxylic acids.

For simplicity, the minor E isoprene resonance branches are neglected as well as the formation of the organic nitrates except for isoprene, MVK and MACR peroxy radicals. There is a clear need for additional constraints regarding the reaction of isoprene nitrates with ozone as well as the photooxidation of 3-methylfuran under high NO_x conditions.

6 Applications of CIMS-based approaches

In this study, we combine chamber measurements by CF_3O^--based CIMS calibrated by theoretically computed dipoles and polarizabilities with the development of a detailed chemical mechanism. The CIMS provides direct and sensitive measurements of a broad range of VOC with high temporal resolution. Its specificity coupled with the small number of ionization channels facilitate the interpretation of the data. The calibrations inferred from quantum chemistry calculations provide additional constraints which help develop a detailed chemical mechanism. Since the CIMS can be used both during laboratory and field experiments, this approach should help provide additional constraints for numerous photooxidation processes as well as chemical transport mod-

els.

Appendix A

Acronyms.

See Table A1.

Appendix B

Calibration

B1 Definitions

We define the normalized signal, $\widehat{\text{Signal}}(m/z)$ as the absolute number of counts recorded at m/z divided by the number of counts associated with the reagent anion, CF_3O^-:

$$\widehat{\text{Signal}}(m/z) = \frac{\text{Signal}(m/z)}{\text{Signal}(CF_3O^-)} \quad \text{(B1)}$$

For the chamber experimental conditions, the reagent ion was found in several forms: CF_3O^-, $CF_3O{\cdot}H_2O$ and $CF_3O^-{\cdot}H_2O_2$. Due to the high count rates for the primary isotopes of the reagent ions (sum$\sim$14 MHz), the ^{13}C isotopes were monitored instead:

$$\text{Signal}(CF_3O^-) = \sum_{m/z=86,104,120} \text{Signal}(m/z) \quad \text{(B2)}$$

As stated in Sect. 2.3, in order to get the concentration for an analyte, X, detected as a product ion with m/z=p, we divide the normalized signal for m/z by the sensitivity (c_X) for that analyte under chamber conditions (Eq. 1).

The above method fails when mass analog ions, i.e. different ions with the same mass-to-charge ratio, exist at the m/z of interest. The mass analog ions correspond to different analytes in the chamber, which have different reaction rate coefficients with the reagent ion. While the CIMS instrument can not separate mass analogs, the explicit model can. To compare the model results with a measured signal composed of mass analogs, we use the following:

$$\left[X_{\text{measured m/z=a}}\right]_{\text{ppbv}} = \frac{\widehat{\text{Signal(m/z)}}}{c_{\text{ref}}} \tag{B3}$$

$$\left[X_{\text{model m/z=a}}\right]_{\text{ppbv}} = \sum_{i \in \mathcal{A}} [X_i] \frac{c_{X_i}}{c_{\text{ref}}} \tag{B4}$$

where **a** is a m/z containing mass analog ions, $\mathcal{A}$ the subset of compounds yielding product ions with m/z=a and $c_{\text{ref}} = 3.85 \times 10^{-4}$ pptv^{-1} is taken as an approximate general calibration. Nominally, $Signal(CF_3O^-)$=120 kcounts/s, this gives c_{ref}=46 counts.s^{-1}.pptv^{-1}, in the CIMS flow tube. Including the dilution factor (13.2), the sensitivity is 3.5 counts.s^{-1}.pptv^{-1} in the chamber air.

B2 Dipoles and polarizabilities computed by quantum mechanics

The dipole moment and polarizability of a molecule depend on its charge distribution. Thus, different conformers of a molecule can have very different dipole moments. The polarizability is essentially determined by the number of electrons and so is not significantly altered by conformers.

We have calculated the dipole moment and polarizability using density functional theory. Many of the molecules of interest have a large number of structural conformers and we have calculated a conformer distribution for all molecules. To generate the initial set of conformers, we have allowed 3 fold rotation about all CC, CO, CN single bonds. This leads to, for example 162 guess structures in the MNBOLZ(1, 4) nitrate.

For each guess conformer, geometry optimization is conducted at the B3LYP/6-31G(d) level. The optimized conformers are ranked by energy and relative population for a temperature of 298 K is determined. We have only calculated the polarizability of the lowest energy structure for each of the molecules as we found this to be relatively insensitive to structure.

Test calculations on a few small molecules for which the dipole moment has been measured show that the B3LYP/6-31G(d) calculated dipole moments are in reasonably good agreement with experiment. The worst agreement is for glycolaldehyde for which the experimental dipole is ~20% larger than the calculated value. Calculations with a larger basis set [B3LYP/6-311+G(d,p)] improved the agreement for glycolaldehyde but lead to worse agreement for other examples. Comparison of results with the B3LYP and the correlated CCSD methods gave very similar dipole moments for glycolaldehyde for a range of basis sets from 6-31G(d) to a reasonably large aug-cc-pVTZ basis set. All calculations were performed with Spartan'06, with the default convergence criteria (Wavefunction Inc., 2006).

B3 Accuracy

In this study, we have assumed that ligand exchange has a negligible impact on CIMS sensitivity. Therefore to assess the accuracy of our calibration, we compare the calculated collision rate with the fastest experimental collision rate:

$$k^r_X = \frac{c^e_X}{c_{\text{HNO}_3}} k^r_{\text{HNO}_3} \tag{B5}$$

where $k^r_{\text{HNO}_3} = 2.2 \times 10^{-9}$ cm^3 molecule^{-1} s^{-1} (Huey et al., 1996; Amelynck et al., 2000) and c^e_X is the maximum sensitivity of this technique determined experimentally by changing the water vapor mixing ratio (often found at zero water vapor mixing ratio).

The sensitivity of the CIMS to strong acids such as nitric acid ($r = \frac{k_X . k^r_{\text{HNO}_3}}{k_{\text{HNO}_3} k^r_X} = 0.9$) or representative VOC such as glycolaldehyde, (r=0.96) appears to be correctly cap-

tured using the thermal collision rate. Furthermore in a recent study, Ng et al. (2008) monitored the oxidation of isoprene by NO_3 using CIMS. Using the dipoles and the polarizabilities of ISOPN(4, 1), MNBOL(1, 4) and MNBL(1, 4) (Table C), we infer that they account for 100% of the carbon flux, consistent with previous determination.

Conversely, the sensitivity to smaller molecules such as formic (r=1.5) or acetic acid (r=2) is largely overpredicted. If the experimental rates of Amelynck et al. (2000) are used, the agreement is much better with r=1.0 for formic acid and r=1.1 for acetic acid. The discrepancy may be explained by the smaller collisional energy used in the latter experiment which would result in fewer A^-.HF complexes being broken.

Furthermore, ligand exchange is not negligible for these small acids and the calibration should take into account both water vapor mixing ratio and hydrogen peroxide. Since the reaction of the cluster $CF_3O^-.H_2O_2$ with both acid (HA) yields only CF_3O^-.HA, we normalize the fluoride transfer signal for formic, $HCOO^-$.HF (m/z=65) and acetic acid, CH_3COO^-.HF (m/z=79), using Signal(CF_3O^-)−Signal(120) in order to eliminate the contribution of hydrogen peroxide. Calibrations for formic and acetic acid transfers derived in the laboratory for various water concentrations can then be used to infer the concentration of both acids. The final result is scaled down by 20%. The uncertainty in the calibration of the small acids is on the order of ±20%.

Appendix C

Inorganic chemistry uncertainties

Proper modeling of the background chemistry is needed to derive conclusions regarding the VOC chemistry. The model is especially sensitive to the following parameters:

Nitric acid. The rate of $HO + NO_2 + M \rightarrow HNO_3$ is an important uncertainty regarding the background chemistry. We use the recently reported rate coefficient of 9.16×10^{-12} cm^3 molecule^{-1} s^{-1} (Okumura and Sander, 2005) which tends to lower the rate of formation of nitric acid and conversely increases the formation rate of ozone in comparison with the previous estimates (Atkinson et al., 2006).

Dinitrogen Pentoxide. N_2O_5 is known to react with water on surfaces (aerosol, walls) to yield nitric acid:

$$N_2O_5 + H_2O \xrightarrow{\mathcal{S}} 2HNO_3 \quad \text{(R23)}$$

The estimated N_2O_5 profile, obtained by removing the nitric acid contribution (m/z=82) to the NO_3^- (m/z=62) signal (Huey et al., 1996), provides evidence for Reaction (R23) in the chamber. The DMA measurements can be used to obtain the aerosol surface area $\mathcal{S}$ and the collision rate, $k_{coll} = \frac{1}{4}\sqrt{\frac{8RT}{\pi M}}\mathcal{S} = 2 \times 10^{-3}$ cm^3 molecule^{-1} s^{-1} . The accommodation coefficient is set to 0.15.

Initial concentration of H_2O_2. Due to the technique used in this experiment to introduce H_2O_2 into the chamber, its concentration is not known accurately. No calibration is available at such a high hydrogen peroxide level, so that its estimate based on CIMS measurement is uncertain: 1.9–2.3 ppm.

Despite these uncertainties, a satisfactory representation for the background chemistry species is reached (Figs. C1 and C2). In particular, HO_2NO_2, a very sensitive marker for the ratio of NO_x and HO_x, is well captured during the first and second regimes. Furthermore we evaluate the skill of the model using the relative peak times (Δt) and maximum intensities (Δc) for various species, which span a wide range of sources and therefore provide strong constraints on the mechanism. The mechanism captures correctly the peak times indicating that the chemical speed is properly modeled in the first and second regime. The error regarding the maximum intensity falls within the uncertainty pointed out in the previous section. The sensitivity of the CIMS to PNA is probably underevaluated due to ligand exchange with H_2O_2.

Acknowledgements. F. Paulot wishes to thank C. D. Vecitis for helpful discussions regarding chemical mechanisms. This study was supported by the National Science Foundation (NSF) under grant ATM-0432377, by the US department of energy under grant DE-FG02-05ER63982,

by US EPA under grant RD-83374901 and by the Marsden Fund administrated by the Royal Society of New Zealand. F. Paulot is supported by the William and Sonya Davidow graduate fellowship. J. D. Crounse. thanks the EPA-STAR Fellowship Program (FP916334012) for providing support. This work has not been formally reviewed by the EPA. The views expressed in this document are solely those of the authors and the EPA does not endorse any products or commercial services mentioned in this publication.

References

Amelynck, C., Schoon, N., and Arijs, E.: Gas phase reactions of $CF3O^-$ and $CF3O^-H2O$ with nitric, formic, and acetic acid, Int. J. Mass Spectrom., 203, 165–175, 2000. 14647, 14649, 14678, 14679

Andreae, M. O., Andreae, T. W., Talbot, R. W., and Harriss, R. C.: Formic and acetic acid over the central Amazon region, Brazil. I-Dry season, J. Geophys. Res., 93, 1616–1624, 1988. 14671

Apponi, A. J., Hoy, J. J., Halfen, D. T., Ziurys, L. M., and Brewster, M. A.: Hydroxyacetone (CH_3COCH_2OH): A Combined Microwave and Millimeter-Wave Laboratory Study and Associated Astronomical Search, Astrophys. J., 652, 1787–1795, 2006. 14693

Arey, J., Aschmann, S. M., Kwok, E. S. C., and Atkinson, R.: Alkyl nitrate, hydroxyalkyl nitrate, and hydroxycarbonyl formation from the NO x-air photooxidations of C 5-C 8 n-alkanes, J. Phys. Chem. A, 105, 1020–1027, 2001. 14651, 14652, 14664

Atkinson, R.: Gas-Phase Tropospheric Chemistry of Volatile Organic Compounds: 1. Alkanes and Alkenes, J. Phys. Chem. Ref. Data, 26, 215, 1997. 14654

Atkinson, R., Aschmann, S. M., Tuazon, E. C., Arey, J., and Zielinska, B.: Formation of 3-Methylfuran from the gas-phase reaction of OH radicals with isoprene and the rate constant for its reaction with the OH radical, Int. J. Chem. Kinet., 21, 593–604, 1989. 14662

Atkinson, R., Baulch, D. L., Cox, R. A., Crowley, J. N., Hampson, R. F., Hynes, R. G., Jenkin, M. E., Rossi, M. J., and Troe, J.: Evaluated kinetic and photochemical data for atmospheric chemistry: Volume I-gas phase reactions of O_x, HO_x, NO_x and SO_x species, Atmos. Chem. Phys, 4, 1461–1738, 2004. 14650

Atkinson, R., Baulch, D. L., Cox, R. A., Crowley, J. N., Hampson, R. F., Hynes, R. G., Jenkin, M. E., Rossi, M. J., and Troe, J.: Evaluated kinetic and photochemical data for atmospheric

chemistry: Volume II–gas phase reactions of organic species, Atmos. Chem. Phys., 6, 3625–4055, 2006, http://www.atmos-chem-phys.net/6/3625/2006/. 14650, 14651, 14654, 14662, 14680

Baker, J., Arey, J., and Atkinson, R.: Formation and Reaction of Hydroxycarbonyls from the Reaction of OH Radicals with 1,3-Butadiene and Isoprene, Environ. Sci. Technol., 39, 4091–4099, 2005. 14662

Barnes, I., Becker, K. H., Fink, E. H., Reimer, A., Zabel, F., and Niki, H.: FTIR spectroscopic study of the gas-phase reaction of HO_2 with H_2CO, Chem. Phys. Lett., 115, 1–8, 1985. 14674

Bethel, H. L., Atkinson, R., and Arey, J.: Kinetics and products of the reactions of selected diols with the OH radical, Int. J. Chem. Kinet., 33, 310–316, 2001. 14662

Bierbach, A., Barnes, I., and Becker, K. H.: Product and kinetic study of the OH-initiated gas-phase oxidation of furan, 2-methylfuran and furanaldehydes at $\simeq$ 300 K, Atmos. Environ., 29, 2651–2660, 1995. 14669, 14691

Butkovskaya, N. I., Pouvesle, N., Kukui, A., and Bras, G. L.: Mechanism of the OH-initiated oxidation of glycolaldehyde over the temperature range 233–296 K., J. Phys. Chem. A, 110, 13 492–13 499, 2006a. 14670, 14671

Butkovskaya, N. I., Pouvesle, N., Kukui, A., Mu, Y., and Le Bras, G.: Mechanism of the OH-Initiated Oxidation of Hydroxyacetone over the Temperature Range 236–298 K, J. Phys. Chem. A, 110, 6833–6843, 2006b. 14670, 14671

Cameron, M., Sivakumaran, V., Dillon, T. J., and Crowley, J. N.: Reaction between OH and CH3CHO Part 1. Primary product yields of CH_3 (296 K), CH_3CO (296 K), and H (237–296 K), Phys. Chem. Chem. Phys., 4, 3628–3638, 2002. 14671

Carlton, A. G., Turpin, B. J., Lim, H. J., Altieri, K. E., and Seitzinger, S.: Link between isoprene and secondary organic aerosol (SOA): Pyruvic acid oxidation yields low volatility organic acids in clouds, Geophys. Res. Lett., 33, 6, L06822, doi:10.1029/2005GL025374, 2006. 14672

Carter, W. P. L. and Atkinson, R.: Alkyl nitrate formation from the atmospheric photoxidation of alkanes; a revised estimation method, J. Atmos. Chem., 8, 165–173, 1989. 14651

Chebbi, A. and Carlier, P.: Carboxylic acids in the troposphere, occurrence, sources, and sinks: A review, Atmos. Environ., 30, 4233–4249, 1996. 14669

Chen, X., Hulbert, D., and Shepson, P. B.: Measurement of the organic nitrate yield from OH reaction with isoprene, J. Geophys. Res., 103, 25 563–25 568, 1998. 14663

Chuong, B. and Stevens, P. S.: Measurements of the kinetics of the OH-initiated oxidation of isoprene, J. Geophys. Res., 107, D13, 4162, doi:10.1029/2001JD000865, 2002. 14663
Chuong, B. and Stevens, P. S.: Measurements of the kinetics of the OH-initiated oxidation of methyl vinyl ketone and methacrolein, Int. J. Chem. Kinet., 36, 12–25, 2004. 14667
Claeys, M., Graham, B., Vas, G., et al.: Formation of Secondary Organic Aerosols Through Photooxidation of Isoprene, Science, 303, 1173–1176, 2004. 14644
Cox, A. P., Brittain, A. H., and Finnigan, D. J.: Microwave spectrum, structure, dipole moment and quadrupole coupling constants of cis and trans nitrous acids, T. Faraday Soc., 67, 2179–2194, 1971. 14693
Crounse, J. D., McKinney, K. A., Kwan, A. J., and Wennberg, P. O.: Measurement of gas-phase hydroperoxides by chemical ionization mass spectrometry, Anal. Chem., (Washington, D.C.), 78, 6726–6732, 2006. 14645, 14646, 14647, 14649
Dibble, T. S.: Isomerization of OH-Isoprene Adducts and Hydroxyalkoxy Isoprene Radicals, J. Phys. Chem. A, 106, 6643–6650, 2002. 14661, 14662
Dibble, T. S.: Intramolecular hydrogen bonding and double H-atom transfer in peroxy and alkoxy radicals from isoprene, J. Phys. Chem. A, 108, 2199–2207, 2004a. 14658, 14663
Dibble, T. S.: Prompt chemistry of alkenoxy radical products of the double H-atom transfer of alkoxy radicals from isoprene, J. Phys. Chem. A, 108, 2208–2215, 2004b. 14658, 14663
Dillon, T. J., Horowitz, A., Hölscher, D., Crowley, J. N., Vereecken, L., Peeters, J., and Matter, S.: Reaction of HO with hydroxyacetone ($HOCH_2C(O)CH_3$): rate coefficients (233–363 K) and mechanism, Phys. Chem. Chem. Phys, 8, 236–246, 2006. 14663
Espada, C. and Shepson, P. B.: The production of organic nitrates from atmospheric oxidation of ethers and glycol ethers, Int. J. Chem. Kinet., 37, 686–699, 2005. 14664
Fan, J. and Zhang, R.: Atmospheric Oxidation Mechanism of Isoprene, Environ. Chem., 1, 140–149, 2004. 14662
Fiore, A. M., Horowitz, L. W., Purves, D. W., II, H. L., Evans, M. J., Wang, Y., Li, Q., and Yantosca, R. M.: Evaluating the contribution of changes in isoprene emissions to surface ozone trends over the eastern United States, J. Geophys. Res., 110, D12303, doi:10.1029/2004JD005485, 2005. 14645, 14664
Francisco-Marquez, M., Alvarez-Idaboy, J. R., Galano, A., and Vivier-Bunge, A.: A Possible Mechanism for Furan Formation in the Tropospheric Oxidation of Dienes, Environ. Sci. Technol., 39, 8797–8802, 2005. 14659
Giacopelli, P., Ford, K., Espada, C., and Shepson, P. B.: Comparison of the measured and

simulated isoprene nitrate distributions above a forest canopy, J. Geophys. Res. D. Atmospheres, 110, 2005. 14657, 14664, 14666, 14668, 14674
Guenther, A., Karl, T., Harley, P., Wiedinmyer, C., Palmer, P. I., and Geron, C.: Estimates of global terrestrial isoprene emissions using MEGAN (Model of Emissions of Gases and Aerosols from Nature), Atmos. Chem. Phys., 6, 3181–3210, 2006, http://www.atmos-chem-phys.net/6/3181/2006/. 14644
Harley, P., Vasconcellos, P., Vierling, L., et al.: Variation in potential for isoprene emissions among Neotropical forest sites, Global Change Biology, 10, 630–650, 2004. 14645
Harley, P. C., Monson, R. K., and Lerdau, M. T.: Ecological and evolutionary aspects of isoprene emission from plants, Oecologia, 118, 109–123, 1999. 14644
Hasson, A. S., Tyndall, G. S., and Orlando, J. J.: A product yield study of the reaction of HO_2 radicals with ethyl peroxy ($C_2H_5O_2$), acetyl peroxy ($CH_3C(O)O_2$), and acetonyl peroxy ($CH_3C(O)CH_2O_2$) radicals, J. Phys. Chem., 108, 5979–5989, 2004. 14653
Henze, D. K. and Seinfeld, J. H.: Global secondary organic aerosol from isoprene oxidation, Geophys. Res. Lett., 33, L09812, doi:10.1029/2006GL025976, 2006. 14645
Hermans, I., Müller, J. F., Nguyen, T. L., Jacobs, P., and Peeters, J.: Kinetics of-Hydroxyalkylperoxyl Radicals in Oxidation Processes. HO_2 Initiated Oxidation of Ketones/Aldehydes near the Tropopause, J. Phys. Chem. A, 109, 4303–4311, 2005. 14669
Horowitz, L. W., Liang, J., Gardner, G. M., and Jacob, D. J.: Export of reactive nitrogen from North America during summertime- Sensitivity to hydrocarbon chemistry, J. Geophys. Res., 103, 13 451–13 476, 1998. 14644, 14664
Horowitz, L. W., Fiore, A. M., Milly, G. P., Cohen, R. C., Perring, A., Wooldridge, P. J., Hess, P. G., Emmons, L. K., and Lamarque, J.: Observational constraints on the chemistry of isoprene nitrates over the eastern United States, J. Geophys. Res., 112, 12, doi:10.1029/2006JD007747, 2007. 14664, 14668
Huey, L. G., Villalta, P. W., Dunlea, E. J., Hanson, D. R., and Howard, C. J.: Reactions of $CF3O^-$ with Atmospheric Trace Gases, J. Phys. Chem., 100, 190–194, 1996. 14647, 14649, 14678, 14680
Jacob, D. J. and Wofsy, S. C.: Photochemistry of biogenic emissions over the Amazon forest, J. Geophys. Res., 93, 1477–1486, 1988. 14671
Jenkin, M. E., Hurley, M. D., and Wallington, T. J.: Investigation of the radical product channel of the CH 3 C (O) O 2+ HO 2 reaction in the gas phase, Phys. Chem. Chem. Phys., 9, 3149–3162, 2007. 14653

Johnson III, R. D.: NIST Computational Chemistry Comparison and Benchmark Database NIST Standard Reference Database Number 101 Release 14, http://srdata.nist.gov/cccbdb, 2006. 14693

Karl, M., Dorn, H. P., Holland, F., Koppmann, R., Poppe, D., Rupp, L., Schaub, A., and Wahner, A.: Product study of the reaction of OH radicals with isoprene in the atmosphere simulation chamber SAPHIR, J. Atmos. Chem., 55, 167–187, 2006. 14656, 14658, 14667

Karunanandan, R., Hölscher, D., Dillon, T. J., Horowitz, A., Crowley, J. N., Vereecken, L., and Peeters, J.: Reaction of HO with Glycolaldehyde, $HOCH_2CHO$: Rate Coefficients (240–362 K) and Mechanism, J. Phys. Chem. A, 111, 897–908, 2007. 14663

Kroll, J. H., Ng, N. L., Murphy, S. M., Flagan, R. C., and Seinfeld, J. H.: Secondary organic aerosol formation from isoprene photooxidation, Environ. Sci. Technol., 40, 1869–1877, 2006. 14645, 14646, 14670

Kwok, E. S. C. and Atkinson, R.: Estimation of hydroxyl radical reaction rate constants for gas-phase organic compounds using a structure-reactivity relationship: an update, Atmos. Environ., 29, 1685–1695, 1995. 14650

Lei, W., Zhang, R., McGivern, W. S., Derecskei-Kovacs, A., and North, S. W.: Theoretical Study of OH – O_2-Isoprene Peroxy Radicals, J. Phys. Chem. A, 105, 471–477, 2001. 14656, 14657

Maryott, A. A. and Buckley, F.: US National Bureau of Standards Circular No. 537, National Bureau of Standards, Washington, D.C., 1953. 14693

Méreau, R., Rayez, M. T., Rayez, J. C., Caralp, F., and Lesclaux, R.: Theoretical study on the atmospheric fate of carbonyl radicals: kinetics of decomposition reactions, Phys. Chem. Chem. Phys., 3, 4712–4717, 2001. 14650

Neeb, P.: Structure-Reactivity Based Estimation of the Rate Constants for Hydroxyl Radical Reactions with Hydrocarbons, J. Atmos. Chem., 35, 295–315, 2000. 14663, 14665

Ng, N. L., Kwan, A. J., Surratt, J. D., et al.: Secondary organic aerosol (SOA) formation from reaction of isoprene with nitrate radicals (NO 3), Atmos. Chem. Phys. Discuss, 8, 3163–3226, 2008. 14679

O'Brien, J. M., Czuba, E., Hastie, D. R., Francisco, J. S., and Shepson, P. B.: Determination of the hydroxy nitrate yields from the reaction of C 2–C 6 alkenes with OH in the presence of NO, J. Phys. Chem. A, 102, 8903–8908, 1998. 14652, 14664

Okumura, M. and Sander, S. P.: Gas-Phase Formation Rates of Nitric Acid and Its Isomers under Urban Conditions, California Environmental Protection Agency, Air Ressources Board, 2005. 14679

Orlando, J. J. and Tyndall, G. S.: The atmospheric chemistry of the HC (O) CO radical, Int. J. Chem. Kinet., 33, 149–156, 2001. 14650

Orlando, J. J., Tyndall, G. S., Bertman, S. B., Chen, W., and Burkholder, J. B.: Rate coefficient for the reaction of OH with CH_2 = C(CH3)C(O)OONO$_2$ (MPAN), Atmos. Environ., 36, 1895–1900, 2002. 14705

Papagni, C., Arey, J., and Atkinson, R.: Rate constants for the gas-phase reactions of OH radicals with a series of unsaturated alcohols, Int. J. Chem. Kinet., 33, 142–147, 2001. 14662

Patchen, A. K., Pennino, M. J., Kiep, A. C., and Elrod, M. J.: Direct kinetics study of the product-forming channels of the reaction of isoprene-derived hydroxyperoxy radicals with NO, Int. J. Chem. Kinet., 39, 353, 2007. 14664

Paulson, S. E., Flagan, R. C., and Seinfeld, J. H.: Atmospheric photooxidation of isoprene. I: The hydroxyl radical and ground state atomic oxygen reactions, Int. J. Chem. Kinet., 24, 79–101, 1992. 14658, 14662

Peeters, J., Fantechi, G., and Vereecken, L.: A Generalized Structure-Activity Relationship for the Decomposition of (Substituted) Alkoxy Radicals, J. Atmos. Chem., 48, 59–80, 2004. 14655

Pfister, G. G., Emmons, L. K., Hess, P. G., Lamarque, J. F., Orlando, J. J., Walters, S., Guenther, A., Palmer, P. I., and Lawrence, P. J.: Contribution of isoprene to chemical budgets: A model tracer study with the NCAR CTM MOZART-4, J. Geophys. Res., 113, D05308, doi:10.1029/2007JD008948, 2008. 14675

Roberts, J. M. and Fajer, R. W.: UV absorption cross sections of organic nitrates of potential atmospheric importance and estimation of atmospheric lifetimes, Environ. Sci. Technol., 23, 945–951, 1989. 14654

Rosenstiel, T. N., Potosnak, M. J., Griffin, K. L., Fall, R., and Monson, R. K.: Increased CO_2 uncouples growth from isoprene emission in an agriforest ecosystem, Nature, 421, 256–259, 2003. 14645

Ryzhkov, A. B., Ariya, P. A., and Matter, S.: A theoretical study of the reactions of parent and substituted Criegee intermediates with water and the water dimer, Phys. Chem. Chem. Phys, 6, 5042–5050, 2004. 14670

Sander, S.: Chemical Kinetics and Photochemical Data for Use in Atmospheric Studies Evaluation Number 15, National Aeronautics and Space Administration, Jet Propulsion Laboratory, California Institute of Technology, 2006. 14650

Sanderson, M. G., Jones, C. D., Collins, W. J., Johnson, C. E., and Derwent, R. G.: Effect of

climate change on isoprene emissions and surface ozone levels, Geophys. Res. Lett., 30, 1936, 18, doi:10.1029/2003GL017642, 2003. 14645

Saunders, S. M., Jenkin, M. E., Derwent, R. G., and Pilling, M. J.: Protocol for the development of the Master Chemical Mechanism, MCM v3 (Part A): tropospheric degradation of non-aromatic volatile organic compounds, Atmos. Chem. Phys, 3, 161–180, 2003. 14653

Shallcross, D. E. and Monks, P. S.: New Directions: A role for isoprene in biosphere–climate–chemistry feedbacks, Atmos. Environ., 34, 1659–1660, 2000. 14645

Sprengnether, M., Demerjian, K. L., Donahue, N. M., and Anderson, J. G.: Product analysis of the OH oxidation of isoprene and 1, 3-butadiene in the presence of NO, J. Geophys. Res., 107, 8–8, 2002. 14656, 14658, 14664, 14668

Su, T. and Chesnavich, W. J.: Parametrization of the ion–polar molecule collision rate constant by trajectory calculations, J. Chem. Phys., 76, 5183, 1982. 14648

Surratt, J. D., Murphy, S. M., Kroll, J. H., et al.: Chemical composition of secondary organic aerosol formed from the photooxidation of isoprene, J. Phys. Chem. A, 110, 9665–9690, 2006. 14645

Talbot, R. W., Andreae, M. O., Berresheim, H., Jacob, D. J., and Beecher, K. M.: Sources and sinks of formic, acetic, and pyruvic acids over Central Amazonia: 2. Wet Season, J. Geophys. Res., 95, 799–16, 1990. 14671

Talbot, R. W., Mosher, B. W., Heikes, B. G., Jacob, D. J., Munger, J. W., Daube, B. C., Keene, W. C., Maben, J. R., and Artz, R. S.: Carboxylic acids in the rural continental atmosphere over the eastern United States during the Shenandoah Cloud and Photochemistry Experiment, J. Geophys. Res., 100, 9335–9344, 1995. 14671

van Donkelaar, A., Martin, R. V., Park, R. J., Heald, C. L., Fu, T. M., Liao, H., and Guenther, A.: Model evidence for a significant source of secondary organic aerosol from isoprene, Atmos. Environ., 41, 1267–1274, 2007. 14645

von Kuhlmann, R., Lawrence, M. G., Pöschl, U., and Crutzen, P. J.: Sensitivities in global scale modeling of isoprene, Atmos. Chem. Phys., 4, 1–17, 2004, http://www.atmos-chem-phys.net/4/1/2004/. 14645, 14664

Wall, K. J., Schiller, C. L., and Harris, G. W.: Measurements of the HONO photodissociation constant, J. Atmos. Chem., 55, 31–54, 2006. 14653

Walser, M. L., Park, J., Gomez, A. L., Russell, A. R., and Nizkorodov, S. A.: Photochemical Aging of Secondary Organic Aerosol Particles Generated from the Oxidation of d-Limonene, J. Phys. Chem. A, 111, 1907–1913, 2007. 14670

Wavefunction Inc.: Spartan'06, 2006. 14648, 14678

Wiedinmyer, C., Tie, X., Guenther, A., Neilson, R., and Granier, C.: Future Changes in Biogenic Isoprene Emissions: How Might They Affect Regional and Global Atmospheric Chemistry?, Earth Interactions, 10, 1–19, 2006. 14645

Table 1. Isoprene nitrate kinetic data.

	Molar yield %	α %	k_{OH} $\times 10^{-11}$	k_{O_3} $\times 10^{-17}$	Recycling (cf. text)
ISOPN 1,2	2.3	5.7	1	1	18
ISOPN 1,4 Z	3.2	24	8.5		52
ISOPN 1,4 E	0.56	24	8.5		52
ISOPN 2,1	0.11	5.7	3.4		−10
ISOPN 3,4	0.28	5.7	6.6		52
ISOPN 4,3	1.3	5.7	1.9	1	27
ISOPN 4,1 Z	2.9	24	8.5		68
ISOPN 4,1 E	0.52	24	8.5		68
Weighted Average	11.2				46

Table 2. Modeled molar yield (number of molecules formed per molecule of initial isoprene) in the chamber conditions at 600 min (NO_x titration).

Compound	Molar Yield (%)	Sources
Formic Acid [(a)]	9.9	Glycolaldehyde: 31%, Hydroxyacetone: 14%, ISOPN(1,4) and (3,4): 23%, MVK_N: 12%
Acetic Acid [(b)]	2.9	Hydroxyacetone: 49%
Pyruvic Acid	1.6	MVK+O_3: 15%, MVK_N(m) channel: 82%
MOBA	1.1	Z1 and Z2
MVK_N	4.8	MVK: 66%, ISOPN (4,3): 29% ISOPN (4,3) + O_3: 5%
MACR_N	4.2	MACR: 58%, ISOPN (1,2): 21% ISOPN (1,2) + O_3: 20%
Ethanal Nitrate	1	ISOPN
Propanone nitrate	1	ISOPN
HC5	9.3	Isoprene
DHB	2.7	Isoprene Nitrate
Hydroxyacetone	18	MACR: 28%, MPAN: 7%, ISOPN: 22%
Methylglyoxal	38	MACR: 19%, MVK: 35%, Hydroxyacetone: 22%
Glycolaldehyde	26	MVK: 74%, ISOPN (r): 15%
Glyoxal	7.8	Glycolaldehyde: 32%, MOBA: 6.4 % Dibble+HC5: 19%, $E_{1,4}$: 8.3 %, $Z_{4,1}$: 19 %, MBDL (from 3-MF): 12%
Formaldehyde	157	Isoprene: 41%

Table 3. Reduced isoprene photooxidation mechanism under high NO_x conditions (chemical notations in Table C).

Reaction			k (T=298K) 10^{-11} cm^3 molecule^{-1} s^{-1}
ISOP + HO	→	$ISOPO_2$	10
$ISOPO_2$ + NO	→	0.4 MVK + 0.26 MACR + 0.89 NO_2 + 0.072 $ISOPONO_2^r$ + 0.038 $ISOPONO_2^{nr}$ 0.66 HCHO + 0.095 HC5 + 0.045 3MF[(a)] + 0.09 THC4 + 0.81 HO_2	10
HC5 + HO	→	HC5OO	12
HC5OO + NO	→	NO_2 + 0.214 (GLYC + MGLYX + GLYX + HACET) + 0.295 DHMOB 0.173 MOBA + 0.104 THC4 + 0.896 HO_2	1.15
$ISOPONO_2^r$ + HO	→	$ISOPOONO_2^r$	8.5
$ISOPOONO_2^r$ + NO	→	0.097 MACR_N + 0.296 HCOOH + 0.423 HACET + 0.747 CH_2O + 1.3545 NO_2 0.125 (GLYC + PROPN_N) + 0.355 DHB + 0.704 HO_2 + 0.1275 ETHL_N + 0.296 NO_3	0.81
$ISOPONO_2^{nr}$ + HO	→	$ISOPOONO_2^{nr}$	1.5
$ISOPOONO_2^{nr}$ + NO	→	0.299 GLYC + 0.329 HACET + 0.6835 HCHO + 0.4035 MACR_N + 0.017 ETHL_N 0.0285 PROP_N + 0.661 HO_2 + 0.24 MVK_N + 0.041 HCOOH + 1.27 NO_2 + 0.041 NO_3	0.81
$ISOPONO_2^{nr}$ + O_3	→	0.35 MVK_N + 0.65 MACR_N + CH_2O	1.3×10^{-6}
$ISOPONO_2^r$ + O_3	→	0.52 (HACET + ETHL_N) + 0.48 (GLYC + PROPN_N)[(b)]	1.3×10^{-6}
THC4 + NO	→	NO_2 + HO_2 + 0.5 (HC4 + CH_2O) + 0.26(HACET + GLYX) + 0.24(GLYC + MGLYX) [(c)]	
MVK + HO	→	MVKOO	1.47
MVKOO + NO	→	0.632 (GLYC + $CH_3C(O)OO$) + 0.274 (MGLYX + CH_2O + HO_2) + 0.094 MVK_N 0.906 NO_2	0.81
MVK_N + HO	→	0.7 HCOOH + NO_3 + 0.7MGLYX + 0.3CH_2O + 0.3$CH_3C(O)C(O)OH$	0.56
MACR + HO	→	0.55 MACROO + 0.45 MCO_3	2.95
MACROO + NO	→	0.85 (NO_2 + HO_2)+0.425 (HACET+CO)+0.425 (CH_2O + MGLYX) + 0.15 MACR_N	0.81
MACR_N + HO	→	0.08 ($CH_3C(O)OH$ + CH_2O + NO_3) + 0.07 (HCOOH + NO_3 + MGLYX) 0.85 (HACET + NO_2) + 0.93 CO_2	5
MC(O)OO + NO	→	NO_2 + CO + CO_2 + CH_2O + CH_3OO	2.1
GLYC + HO	→	0.75 HO_2 + 0.25 HO + 0.13 GLYX + 0.52 CO + 0.35 CO_2 + 0.16 HCOOH + 0.71CH_2O	0.8
HACET + HO	→	0.75 MGLYX + 0.825 HO_2 + 0.125 HCOOH + 0.1 HO + 0.125 CH_3OO + 0.20 CO_2 0.05 CO + 0.125 $CH_3C(O)OH$	0.6
ETHL_N + HO	→	CH_2O + CO_2 + NO_2	1
HC4 + HO	→	HC4OO	4.5
HC4OO + NO	→	CO_2 + HC3OO + NO_2	2
HC3OO + NO	→	CH_2O + $CH_3C(O)OO$ + NO_2	0.81
DHMOB + HO	→	1.5 CO + 0.5 HO_2 + 0.5 HACET + 0.5 HC4s	1
HC4s + HO	→	CO + MGLYX + HO_2	2.55
MOBA + HO	→	HC4s + CO_2 + HO_2	0.3
MPAN + HO	→	0.25 HACET + 0.75 (CH_2O + HO_2 + $CH_3C(O)OO$) + CO_2 + NO_3	2.9

(a): no decomposition scheme proposed (cf. Bierbach et al., 1995), (b): no constraint from this study (cf. text), (c): The two RO_2 + NO reactions of Dibble's mechanism are lumped into one reaction.

Table A1. Chemical notation.

Abbreviation	Formula	IUPAC name (common name)	CAS number
3-MF	C_5H_6O	3-Methylfuran	930-27-8
DHB	$C_4H_8O_3$	Dihydroxybutanone	57011-15-1
DHMOB (1,4)	$C_5H_8O_4$	2,4-dihydroxy-2-methyl-3-oxobutanal	
DHMOB (4,1)	$C_5H_8O_2$	3,4-dihydroxy-3-methyl-2-oxobutanal	
DHPN	$C_3H_6O_3$	Dihydroxypropanone	96-26-4
ETHL_N	$C_2H_3NO_4$	Nitrooxyethanal (ethanal nitrate)	72673-15-5
GLYC	$C_2H_6O_2$	Hydroxyethanal (glycolaldehyde)	141-46-8
GLYX	$C_2H_2O_2$	Ethanedial (glyoxal)	107-22-2
HACET	$C_3H_6O_2$	Hydroxypropanone (hydroxyacetone)	116-09-6
HC5 E(4,1)	$C_5H_8O_2$	(E)-hydroxy-3-methylbutenal	
HC5 Z(1,4)	$C_5H_8O_2$	(Z)-hydroxy-2-methylbutenal	519148-47-1
HC5 Z(4,1)	$C_5H_8O_2$	(Z)-hydroxy-3-methylbutenal	519148-44-8
HMPL	$C_4H_6O_2$	2-(hydroxymethyl)prop-2-enal	40364-84-9
HOPL	$C_3H_4O_3$	Hydroxyoxopropanal	997-10-4
ISOPN (1,2)	$C_5H_9NO_4$	2-methyl-2-(nitrooxy)butenol	227607-01-4
ISOPN (1,4)	$C_5H_9NO_4$	Z-2-methyl-4-(nitrooxy)but-2-en-1-ol	227606-97-5
		E-2-methyl-4-(nitrooxy)but-2-en-1-ol	227606-98-6
ISOPN (2,1)	$C_5H_9NO_4$	2-methyl-1-(nitrooxy)but-3-en-2-ol	227607-02-5
ISOPN (3,4)	$C_5H_9NO_4$	3-methyl-1-(nitrooxy)but-3-en-2-ol	601487-80-3
ISOPN (4,1)	$C_5H_9NO_4$	Z-3-methyl-4-(nitrooxy)but-2-en-1-ol	227606-99-7
		E-3-methyl-4-(nitrooxy)but-2-en-1-ol	227607-00-3
ISOPN (4,3)	$C_5H_9NO_4$	3-methyl-2-(nitrooxy)but-3-en-1-ol	227606-96-4
MACR	C_4H_6O	2-methy-2-propenal (methacrolein)	78-85-3
MACR_N	$C_4H_7NO_5$	4-hydroxy-3-(nitrooxy)-3-methyl-propanal	
MACR_N (m)	$C_4H_7NO_5$	3-hydroxy-4-(nitrooxy)-3-methyl-propanal	
MGLYX	$C_3H_4O_2$	Oxopropanal (methylglyoxal)	78-98-8
MHBL	$C_5H_8O_3$	hydroxy-3-(hydroxymethyl)butenal	535967-80-7
MNBL Z(1,4)	$C_5H_7O_2$	(2Z)-3-methyl-4-(nitrooxy)but-2-enal	227607-07-0
MNBL Z(4,1)	$C_5H_7O_2$	(2Z)-2-methyl-4-(nitrooxy)but-2-enal	227607-05-8
MNBOL Z(1,4)	$C_5H_8O_3$	(2Z)-3-methyl-4-(nitrooxy)but-2-ene-1-peroxol	184243-82-1
MNBOL Z(4,1)	$C_5H_8O_3$	(2Z)-2-methyl-4-(nitrooxy)but-2-ene-1-peroxol	
MOBA Z(1,4)	$C_5H_6O_3$	(Z)-2-methyl-oxobutenoic acid	63170-47-8
MOBA Z(4,1)	$C_5H_6O_3$	(Z)-3-methyl-oxobutenoic acid	70143-04-3
MPDL	$C_4H_6O_2$	Methylpropandial	16002-19-0
MVK	C_4H_6O	Butenone (methylvinylketone)	78-94-4
MVK_N	$C_4H_7NO_5$	4-hydroxy-3-(nitrooxy)butanone	
MVK_N (m)	$C_4H_7NO_5$	3-hydroxy-4-(nitrooxy)butanone	
OBL	$C_4H_6O_2$	3-oxobutanal	625-34-3
PROPN_N	$C_3H_5NO_4$	Nitrooxypropanone (propanone nitrate)	6745-71-7

Table B1. Weighted average dipoles ($\overline{\mu}$) and polarizabilities (α). Experimental determinations are indicated in parenthesis when available. k_X, is the weighted average of the collision rates calculated for conformers with an abundance greater than 5%. k_{HNO_3}=1.92×10^{-9} cm^3 molecule^{-1} s^{-1} . σ is the weighted standard deviation of the distribution of thermal collision rate constants, i.e. it indicates the sensitivity of the calibration to the calculated distribution of conformers.

Molecule (X)	$\overline{\mu}$(D)	α (A^{-3})	k_X/k_{HNO_3}	σ
Acetic Acid	1.6 (1.7°)	3.9 (5.1®)	0.80 (0.84)	ø
DHB	2.3	7.5	1.0	0.027
DHMOB14	1.5	9.3	0.79	0.26
DHMOB41	1.1	9.1	0.66	0.12
DHPN	1.5	6.0	0.74	ø
ETHL_N	2.7	6.2	1.1	0.4
Formic Acid	1.4 (1.4°)	2.4 (3.3°)	0.76 (0.78)	ø
GLYC	2.3 (2.7°)	4.5	1.1 (1.3)	ø
HACET	3.1 (3.1 †)	5.5	1.4 (1.4)	0.72×10^{-3}
HC5 E(4,1)	2.8	8.9	1.2	0.22
HC5 Z(1,4)	3.5	8.7	1.5	0.14
HC5 Z(4,1)	3.7	8.9	1.5	ø
HOPL	1.2	5.7	0.65	1.6×10^{-3}
ISOPN (1,2)	2.5	11	1.0	0.032
ISOPN (2,1)	2.5	11	1.0	0.17
ISOPN (3,4)	2.4	11	1.0	0.11
ISOPN (4,3)	2.5	11	1.0	0.068
ISOPN (1,4)E	3.2	11	1.3	0.17
ISOPN (4,1)E	2.9	12	1.2	0.085
ISOPN (1,4)Z	3.2	11	1.3	0.028
ISOPN (4,1)Z	3.0	11	1.2	0.041
MACR_N(m)	2.4	9.9	1.0	0.38
MACR_N	2.0	9.8	0.87	0.045
MNBL Z(1,4)	3.6	11	1.4	0.089
MNBL Z(4,1)	3.9	12	1.5	0.12
MNBOL Z(1,4)	4.3	12	1.6	0.073
MNBOL Z(4,1)	4.2	12	1.6	0.083
MOBA Z(1,4)	4.6	9.1	1.8	0.22
MOBA Z(4,1)	3.2	9.2	1.3	ø
MVK_N(m)	2.2	9.7	0.95	0.39
MVK_N	2.3	9.9	0.95	0.078
PROPN_N	3.0	7.7	1.3	0.46
Propanoic Acid	1.5	5.4	0.76	0.034
Pyruvic Acid	2.4	5.5	1.0	ø

°: Johnson III, R. D. (2006), †: Apponi et al. (2006), *: Cox et al. (1971)
®: Maryott and Buckley (1953)

Table C1. Skill of the model. $\Delta t = t_{max}^{model}/t_{max}^{data} - 1$ and $\Delta c = c_{max}^{model}/c_{max}^{data} - 1$.

	HACET	GLYC	ISOPN	MVKN	HC5	ETHN	DHB	DHPN	HONO	PNA
Δt (%)	4.4	<1	<1	<1	<1	1.7	1.2	<1	17	−12
Δc_{max} (%)	2.8	<1	<1	−4	30	−11	3.6	7.7	1.8	−37

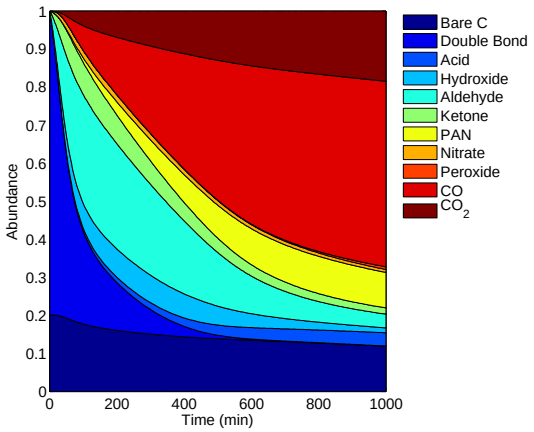

Fig. 1. Evolution of the speciation during isoprene photooxidation. The abundance of a functional group, x, is defined as the sum of the carbons bearing x normalized by the total amount of carbon in the chamber, i.e. five times the initial amount of isoprene.

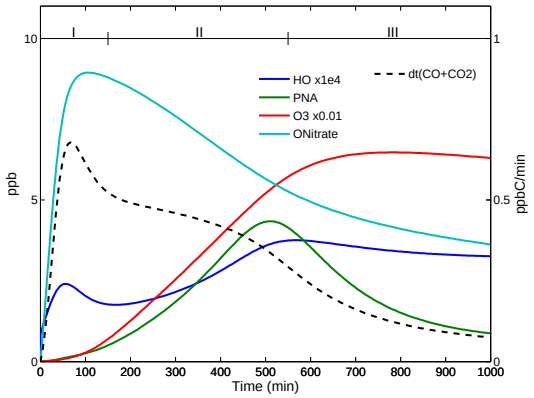

Fig. 2. Different stages of the reaction. Regime I: alkenes chemistry, NO_X-dominated. Regime II: aldehydes chemistry, NO_X-dominated. Regime III: ketones and peroxides chemistry, HO_X-dominated.

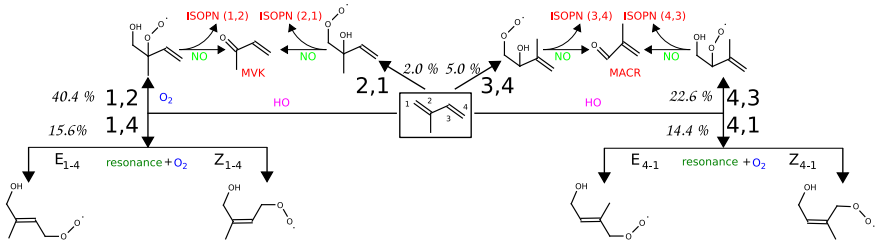

Fig. 3. Addition of HO on isoprene.

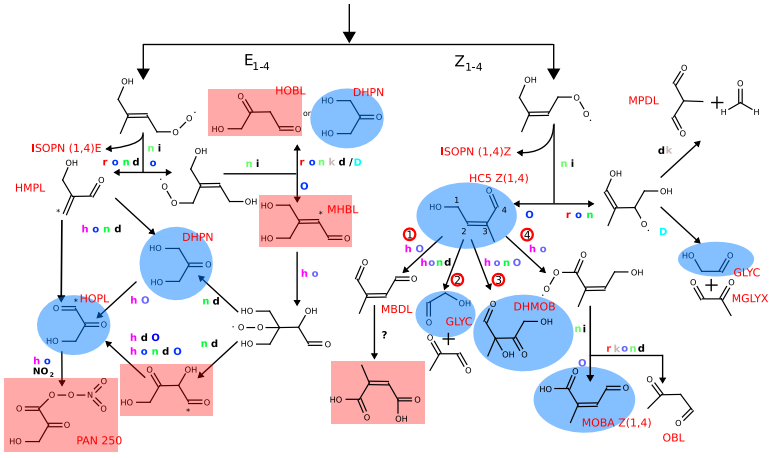

Fig. 4. (1,4) resonance branch. i: δ_1^5 isomerization Reaction (R16), h: HO + VOC (abstraction or addition) $*$ denotes the location of the reaction, o: $R + O_2 \rightarrow RO_2$, O: Reaction (R15), D: Dibble mechanism (cf. Sect. 4.3.1), n: RO_2 + NO Reaction (R7), r: resonance, d: decomposition Reaction (R14), k: keto-enol tautomerism. Blue circles: detected and correctly captured by the model. Red square: Insufficient data/model discrepancy. The formation of 3-methylfuran is depicted in Sect. 4.3.1.

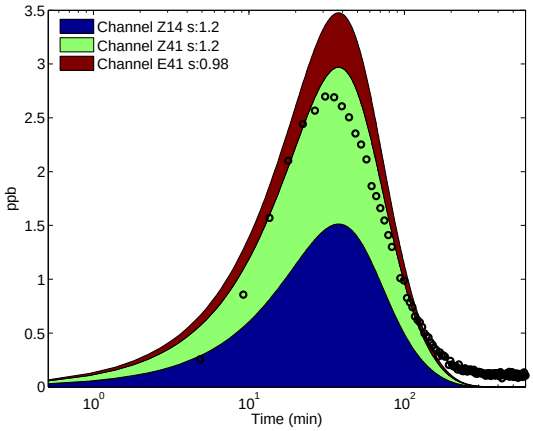

Fig. 5. Source distribution of HC5 (m/z=185).

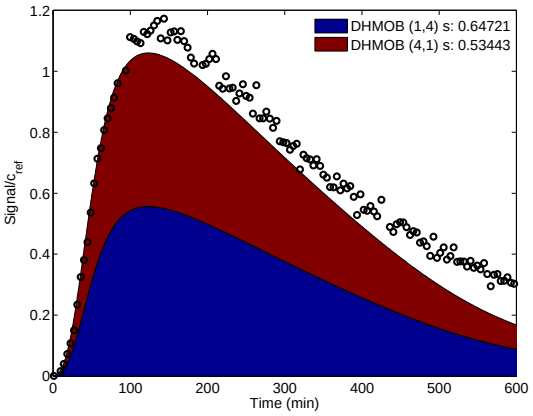

Fig. 6. Source distribution of DHMOB (m/z=217).

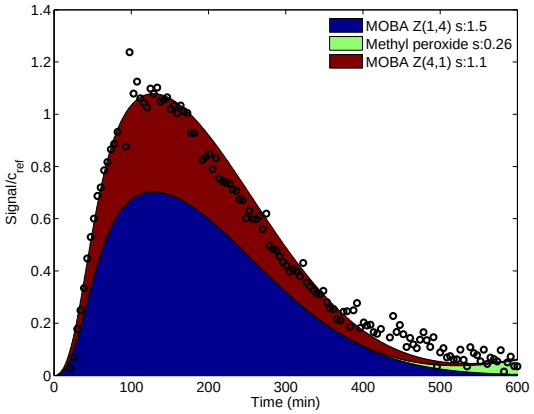

Fig. 7. Source distribution of MOBA (m/z=133 + 199) and Methylperoxide.

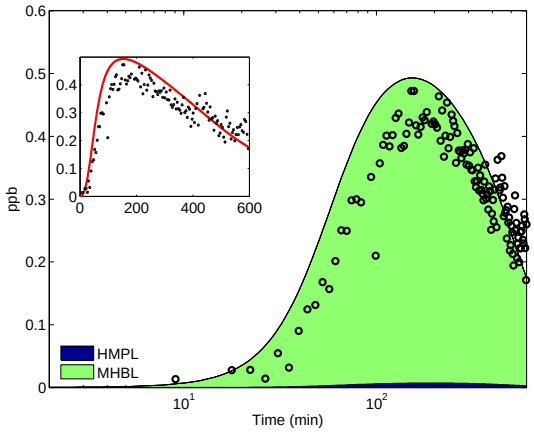

Fig. 8. Source distribution of pyruvic acid and DHPN (m/z=175).

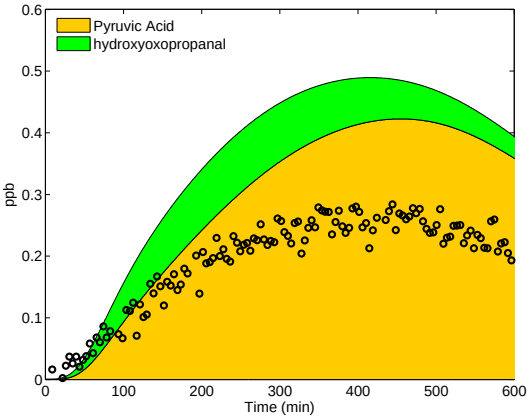

Fig. 9. Source distribution of HOPL (m/z=173).

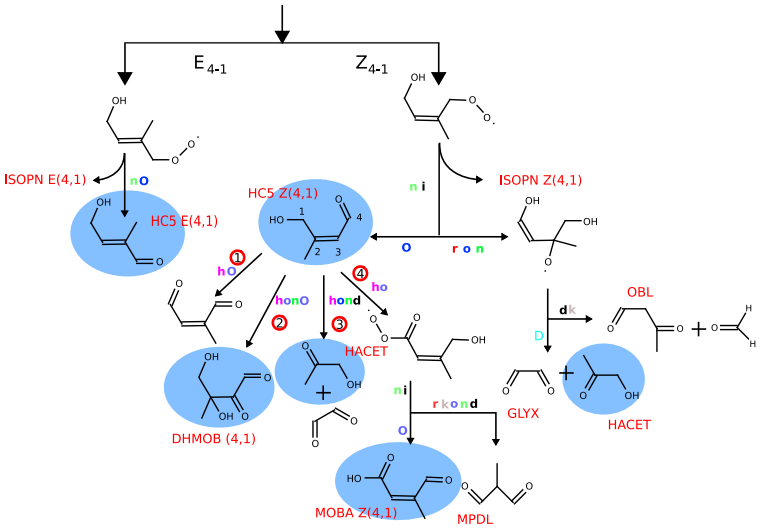

Fig. 10. (4,1) resonance branch. Notations are described in the caption of Fig. 4.

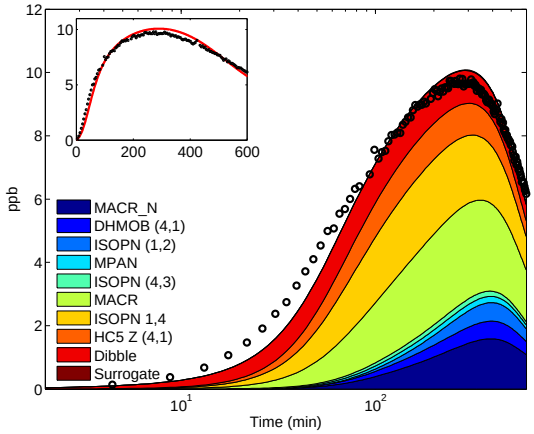

Fig. 11. Source distribution of HACET (m/z=159). MPAN source has been described by Orlando et al. (2002).

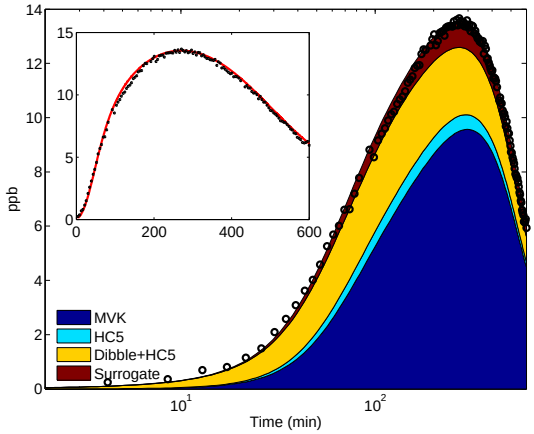

Fig. 12. Source distribution of GLYC (m/z=145 corrected for acetic acid.

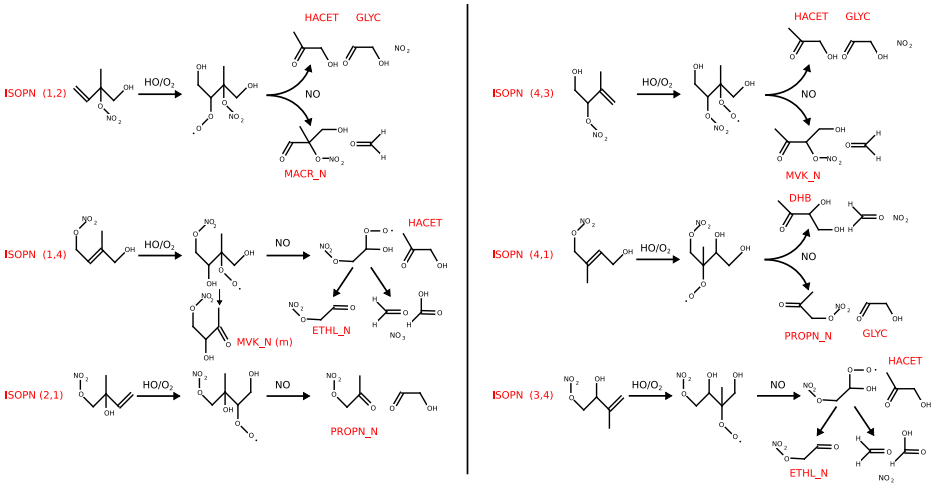

Fig. 13. Decomposition pathway of the different isoprene nitrates after their reaction with HO. The reaction of the isoprene peroxy nitrate with NO also yields an isoprene dinitrate through Reaction (R7).

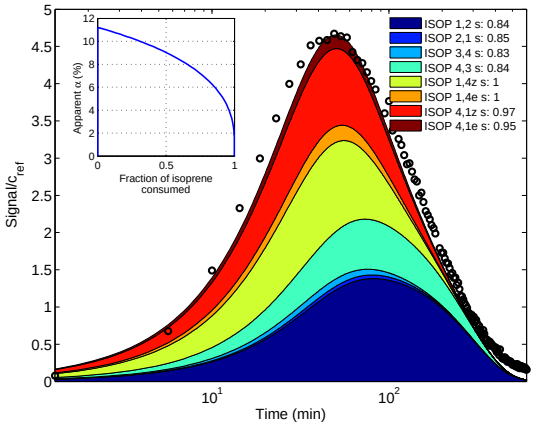

Fig. 14. Isoprene Nitrates (m/z=232).

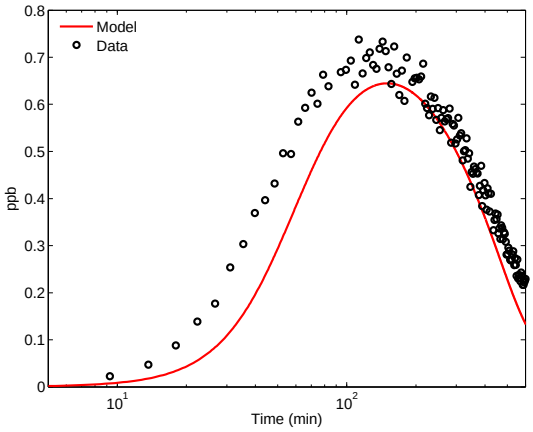

Fig. 15. ETHL_N (m/z=190).

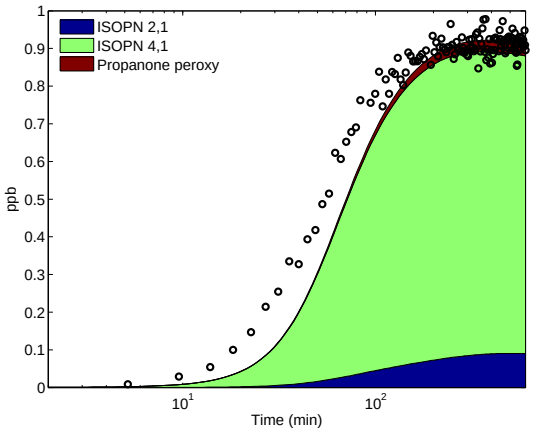

Fig. 16. Source distribution of PROPN_N (m/z=204).

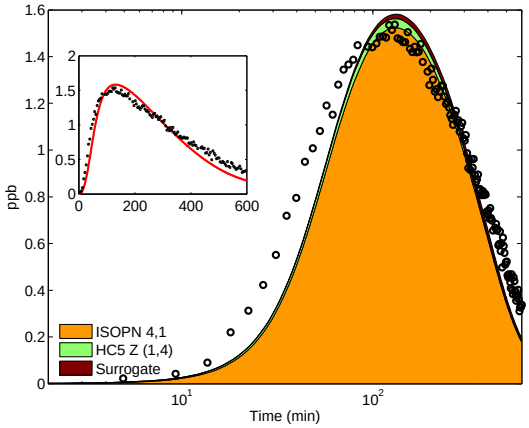

Fig. 17. Source distribution of of DHB (m/z=189).

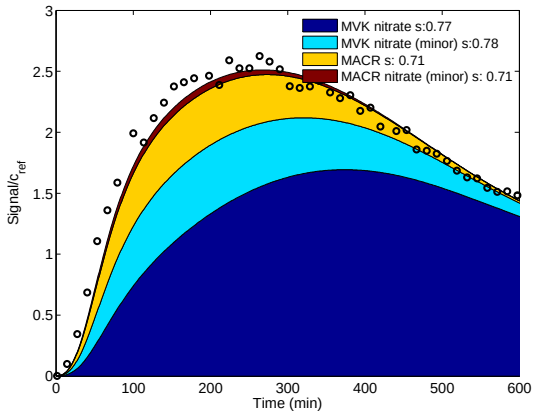

Fig. 18. MVK_N/MACR_N (m/z=234).

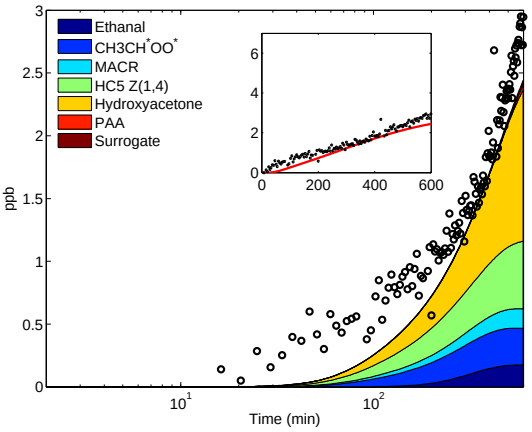

Fig. 19. Source distribution of acetic Acid (m/z=79).

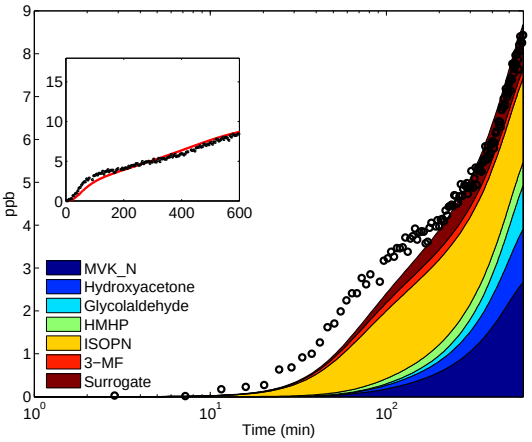

Fig. 20. Source distribution of formic acid (m/z=65).

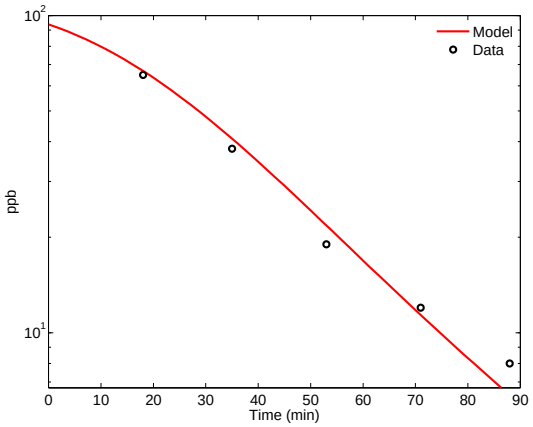

Fig. C1. Isoprene.

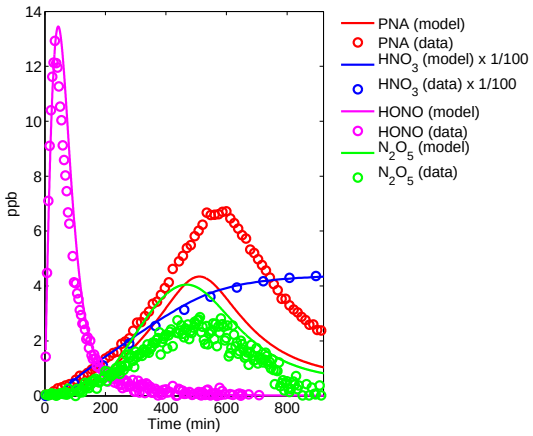

Fig. C2. Background chemistry.